ZONE GENERATOR

FOR

LARGE SPACE TELESCOPE TECHNOLOGY

(NASA-CR-132471) ZONE GENERATOR FOR LARGE SPACE TELESCOPE TECHNOLOGY Final Report (Keuffel and Esser Co.) ~~46~~ 47 p HC $5.50 CSCL 20F

N74-30119

Unclas

G3/23 54564

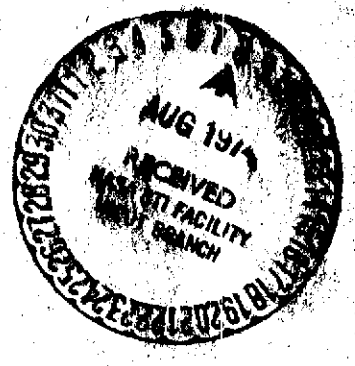

NASA CR132471

F I N A L R E P O R T

ZONE GENERATOR

FOR

LARGE SPACE TELESCOPE TECHNOLOGY

BY: DR. KENT E. ERICKSON

PREPARED UNDER CONTRACT NAS1-11483

KEUFFEL & ESSER COMPANY
MORRISTOWN, NEW JERSEY

NATIONAL AERONAUTICS & SPACE ADMINISTRATION
LANGLEY RESEARCH CENTER
HAMPTON, VIRGINIA

JUNE 19, 1974

I

TABLE OF CONTENTS

		PAGE
1.	SUMMARY	1
2.	INTRODUCTION	1
3.	SYSTEM DESIGN	9
3.1	Turntable	9
3.2	Carriage Support Frame	14
3.3	Radial Motion	14
3.4	Laser Stylus	15
3.5	Mirror	19
3.6	Focus Control	19
4.	PERFORMANCE	25
4.1	Rotary Motion	25
4.2	Radial Motion	25
4.3	Focus Control	25
5.	SCRIBING EXPERIMENTS	26
6.	DISCUSSION	40
7.	CONCLUSIONS	42
8.	ACKNOWLEDGMENTS	42

F I G U R E S

FIGURE #		PAGE
1	MONITORING CONCEPT	2
2	INTERFEROMETRIC RADIAL SENSOR	4
3	ZONE PROFILES	6
4	ZONE GENERATOR SYSTEM	8
5	STATOR AND LATERAL BEARING	10
6	ROTOR AND AXLE	11
7	AIR BEARING MODULE	12
8	MODULE DESIGN	13
9	ZONE GENERATOR	16
10	TURNTABLE AND CARRIAGE	17
11	CARRIAGE DRIVE	18
12	CARRIAGE AND FOCUS CONTROL ASSEMBLIES	20
13	CARRIAGE AND FOCUS CONTROL ARM	21
14	FOCUS SENSOR ASSEMBLY	22
15	FOCUS CONTROL SCHEMATIC	23

FIGURES

FIGURE #		PAGE
16	ZINC	28
17	MAGNESIUM FLUORIDE UNDER ZINC	29
18	MAGNESIUM FLUORIDE OVER ZINC	29
19	TRANSMISSION AND REFLECTION OF SELENIUM	31
20	CHROMIUM ON A SELENIUM MASK-AFTER HEATING	32
21	CHROMIUM LINE	33
22	SELENIUM ON ALUMINUM	34
23	SELENIUM ON CHROMIUM (315X)	35
24	SELENIUM ON CHROMIUM (2100X)	36
25	GALLIUM NITRIDE	37
26	CHROMIUM	38

1.0 SUMMARY

This investigation is aimed at demonstrating the practicality of generating concentric zones in low relief on very large mirrors for the purpose of monitoring the optical performance of large space telescopes. A 1.2m diameter turntable with a "laser stylus" has been constructed to operate at speeds up to 30 r.p.m. The focus of the "laser stylus" is under closed loop control. Scribing experiments were conducted to generate narrow zones with "square wave" profiles. Attempts to use masking layers of selenium and other materials which evaporate without melting were not successful in layers of quarter-wave (160nm) thickness. Generation of zones in lower relief (< 15nm) on mirrors 3m to 4m in diameter appears to be entirely feasible.

2.0 INTRODUCTION

This investigation pursues a concept for monitoring the optical adjustment of a Large Space Telescope (LST) that has evolved through two previous investigations [1] [2]. Since its inception in 1966, the basic premise of this concept has been that the mirrors of an LST would be monolithic and that a slight amount of active control of the mirrors would be preferable to a large amount of active control or to no active control at all.

If active control is provided, a monitoring system is needed. Such a monitoring system should combine high sensitivity with long term stability. Furthermore, it should monitor the alignment and focus of the telescope as well as the figure of the primary mirror.

The monitoring concept is illustrated in Fig. 1. Monitoring light emanates from a C.W. uniphase source (e.g., a 1 milliwatt He-Ne laser) located in the vicinity of the focal plane of the telescope. The monitoring light is split into a monitoring wave and a reference wave. As the

---

(1) Contract NASW-1856; Final Report NASA CR-111911 "Investigation, Monitoring and Control of Large Telescope Performance"; Sept. 1970.

(2) Contract NASI-10564; Final Report NASI-10564 "Fabrication and Evaluation of a Weak Zone Plate for Monitoring Performance of Large Space Telescopes"; July 15, 1972.

MONITORING CONCEPT

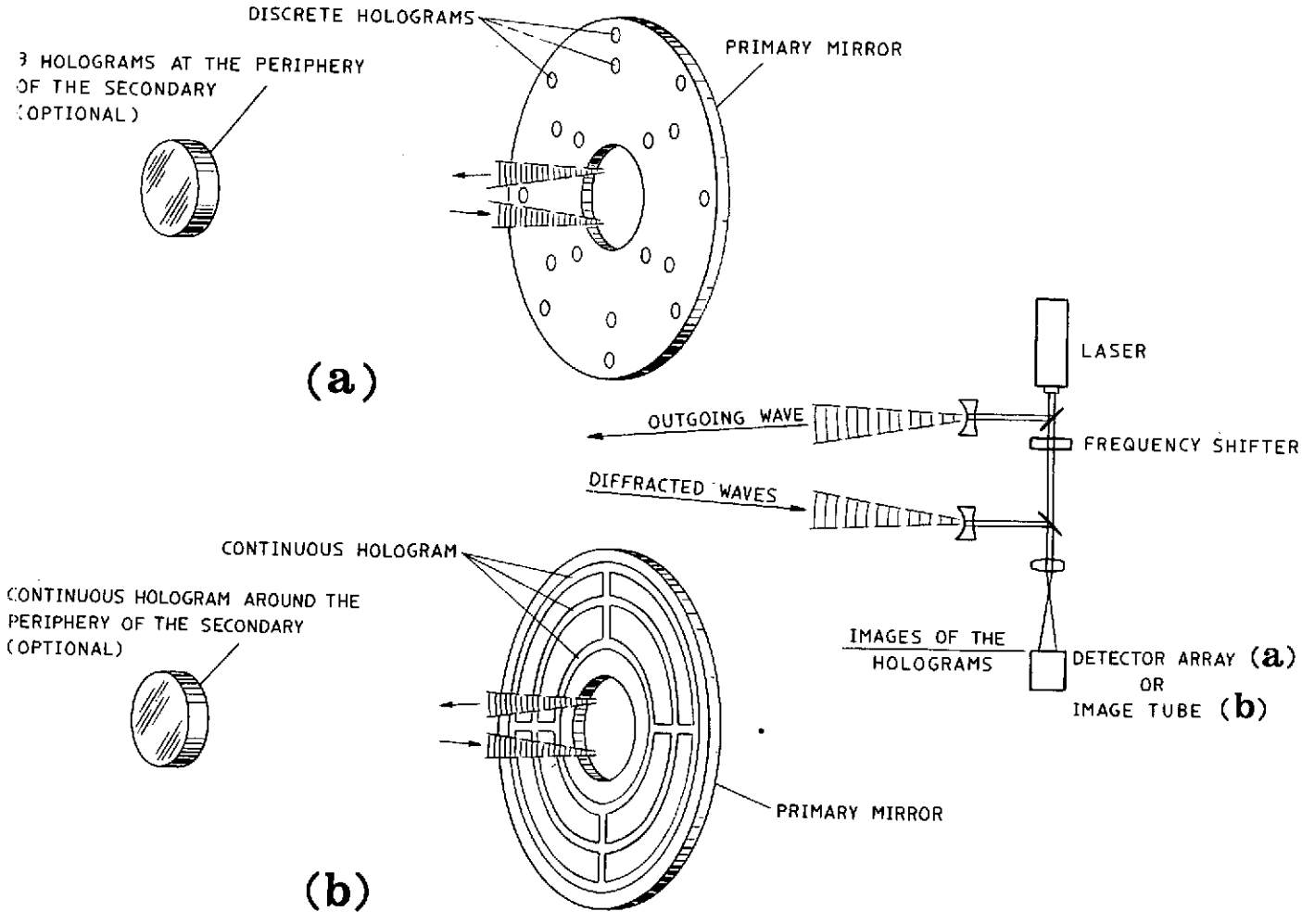

FIGURE 1

monitoring wave traverses the telescope, small portions of it are weakly diffracted from holograms imprinted in very faint relief on portions of the primary mirror. Alignment of the secondary mirror may likewise be monitored by placing holograms at its periphery. The light wave diffracted from each hologram returns through the telescope to the focal plane where it recombines with the reference wave and impinges on a detector. The frequency of the reference wave is shifted so as to convert optical phase differences between the diffracted waves into electrical phase differences between the detector outputs. This phase information is supplied to the active control system.

The sensitivity of this monitoring system arises from its acceptance of phase information from the maximum usable aperture, namely the aperture subtended by the mirrors themselves. The stability of the system arises from the fact that the monitoring wave traverses the system in almost the same manner as starlight.

Two embodiments of the holographic monitoring concept are shown in Fig. 1. In embodiment (a), the monitor is calibrated in orbit while observing the image quality of a test star by auxiliary means. In embodiment (b), the monitor may be calibrated (to lesser accuracy) prior to launch.

Calibration of the monitor consists of establishing a set of phases for the detector outputs which represent optimum adjustment of the telescope. In embodiment (a) of Fig. 1, the N holograms on the mirror (or mirrors) give rise to N electrical signals with phases $\phi_1, \phi_2, \cdots\cdots, \phi_N$. During in-orbit calibration, the values $\phi_1^\circ, \phi_2^\circ, \cdots\cdots, \phi_N^\circ$ which result in optimum stellar image quality are stored in an on-board memory. Since calibration is infrequent (perhaps monthly) the most suitable star in the heavens may be used for this purpose. Between calibrations, a closed loop, slow response, control system maintains the condition $\phi_i = \phi_i^\circ$. The displacements $\Delta x_1, \Delta x_2, \cdots\cdots, \Delta x_N$ of the control actuators which are needed to correct a phase error $\Delta\phi_j$ are computed on-board from a linear relation $\Delta x_i = \sum_{j=1}^{N} B_{ij} \Delta\phi_j$. Coefficients B_{ij} may be accurately evaluated in orbit by observing the system's inverse response $\Delta\phi_i$ to control actuator displacements Δx_j. Design of the control system should be such that a linear relationship is applicable. It is not necessary, however, that the controls be separated into alignment controls, focus controls, and figure controls; stabilization of the ϕ's stabilizes the entire system.

INTERFEROMETRIC RADIAL SENSOR

THE FRAME TO WHICH THE FRINGECOUNTER IS AFFIXED TILTS ABOUT A HORIZONTAL AXIS THROUGH THE CENTER OF THE REFERENCE SPHERE.
THE CARRIAGE TO WHICH THE RETROREFLECTOR AND SCRIBING LENS ARE AFFIXED SLIDES RADIALLY ON THE FRAME.

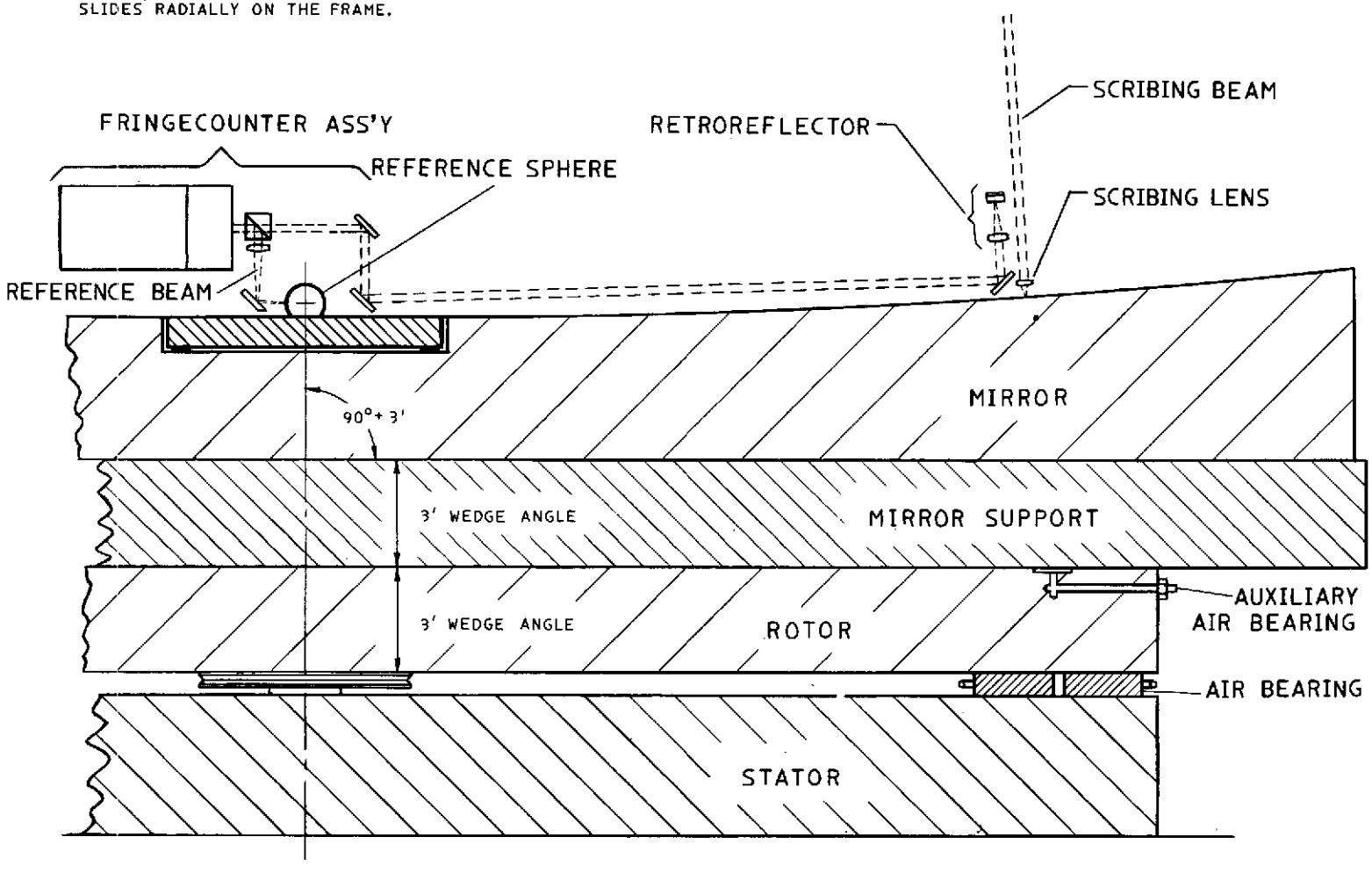

FIGURE 2

In embodiment (b) of Fig. 1 , adjustment of the telescope is monitored via an image tube. In this embodiment, there is continuity of phase information between any two regions within the hologram. The possibility therefore exists of calibrating the monitor absolutely, provided the radii of the circular diffracting zones of the hologram are generated with sufficient accuracy.* Fig. 2 illustrates how these circular zones might be generated under interferometric control on a large turntable without imposing severe requirements on the stability of the turntable. Calibration of the monitor through precision control of the fabrication process would not provide the accuracy attainable through direct stellar checkout. It should suffice, however, to allow a telescope to be assembled in orbit to a tolerance approaching the diffraction limit.

The holograms consist of concentric zones imprinted in relief on the surfaces of the mirrors prior to final overcoating. Fig. 3 shows cross-sectional profiles of two types of zones designed to give low diffraction and scatter. In Type A zones, diffraction and scatter are kept low through the use of a low step height (e.g. 1.5nm). In Type B zones, diffraction and scatter are kept low through the use of fewer zones. With Type A zones, first order diffraction is used for monitoring purposes; with Type B zones, higher order diffraction is used for monitoring purposes. In both cases the spatial period of the zones decreases in the radial direction, so that the desired diffraction order is directed toward the detectors from all portions of the hologram.

Diffraction and scatter of celestial light by the holograms mus not interfere with normal operation of the telescope. Previous investigations (see references on page 1) indicate that holograms satisfactory for monitoring purposes can be so faint and so localized as to have no appreciable adverse effect on stellar images as faint as magnitude 29 in the wavelength region above 100nm.

For the holographic monitoring concept presented above to be practical, a practical means is required for generating the holograms on very large mirrors. Previous investigations (see references on page 1) have tested the concept on mirrors 30cm in diameter on which the holograms were generated photographically. Such methods are not practical for mirrors 3 to 4 meters in diameter. The aim of the present investigation was therefore

---

* For a discussion see reference (1) on page 1.

ZONE PROFILES

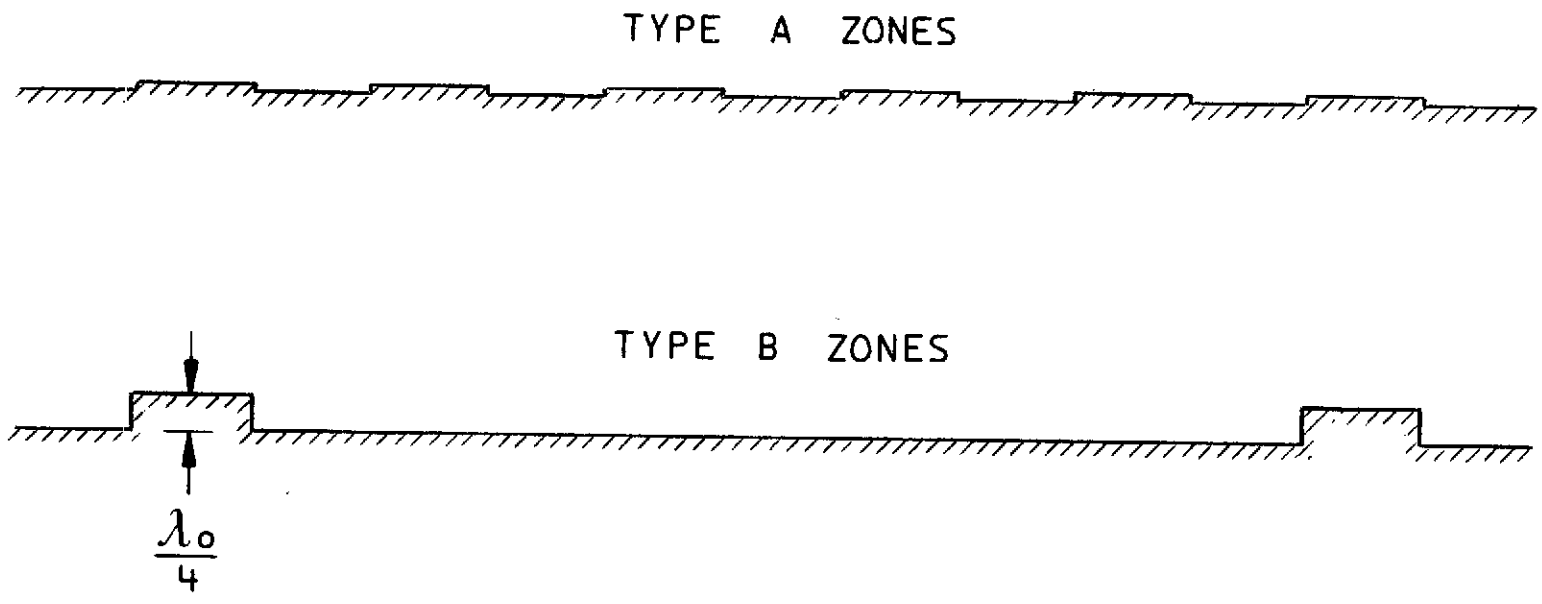

λ_o = WAVELENGTH OF THE MONITORING LIGHT

FIGURE 3

to demonstrate the practicality of scribing the holographic zones on large mirrors using a large turntable and a "laser stylus".

The present investigation had two principal objectives. The first objective was to demonstrate the practicality of the holographic monitoring technique from the standpoint of the design of the turntable and scriber system. The turntable was to have a minimum diameter of 1.2m, a rotary speed controllable within ± 5% up to 30 rev/min, and a "laser stylus" with automatic focus control for maintaining zone quality. Most importantly, the design of the system was to be along lines which could be scaled up to accommodate mirrors at least 3 meters in diameter. Precision radial control was not included in this investigation.

The second objective of this investigation was to develop a technique for scribing zones of suitable depth, width, and uniformity applicable to large telescope mirrors. Emphasis was on Type B zones (see Fig. 3) as these require less cutting time than Type A zones and give less scatter in the far u.v. Zone width was to vary in the range from 1.5 μm to 10 μm at a relief height of approximately 16 nm.

FIGURE 4 ZONE GENERATOR SYSTEM

3.0 SYSTEM DESIGN

3.1 Turntable

3.1.1 Stator

The stator is an octagonal slab of black granite 6 inches thick and 48 inches wide. Flatness tolerances are shown in Fig. 5 . Support is at three points on a circle of 30 inch diameter. The stator is massive enough to support a mirror and mirror mount 2 meters in diameter atop the rotor.

3.1.2 Rotor

The rotor is a circular slab of black granite 6 inches thick and 48 inches in diameter. Flatness tolerances are shown in Fig. 6 . The rotor is wedged so that the axis of a large mirror might be precisely adjusted parallel to the rotor axis by appropriate azimuthal orientation between the mirror, the mirror mount, and the rotor (all similarly wedged as in Fig. 2). The rotor can accommodate a 2 meter mirror mount with an overhang of 38cm.

3.1.3 Air Bearing

Rotor and stator are separated by an air bearing consisting of 24 identical Delrin modules (Fig. 7) distributed uniformly in an annular pattern. In a more massive turntable, modules would be added on a second annulus as indicated in Fig. 2 . The module design is given in Fig. 8 . All modules are machined to the same thickness ± .0002". The bearing operates at an air pressure of 10 psi. At this pressure the air gap is .0012". No lateral constraint was used for the individual modules other than that provided by friction against the stator.

3.1.4 Lateral Bearing

Lateral constraint of the rotor is provided by a teflon friction bearing. The design is shown in Fig. 5 . This bearing mates with a 4 inch diameter axle of polished steel affixed to the underside of the rotor. Contact between the axle and the teflon bearing is maintained by the force of gravity, the plane of the air bearing being inclined by 1^{o} from the horizontal so as to exert a lateral thrust of about 25 lb. This is augmented by a contact force of about 5 lb. between the drive wheel and the rotor.

STATOR AND LATERAL BEARING

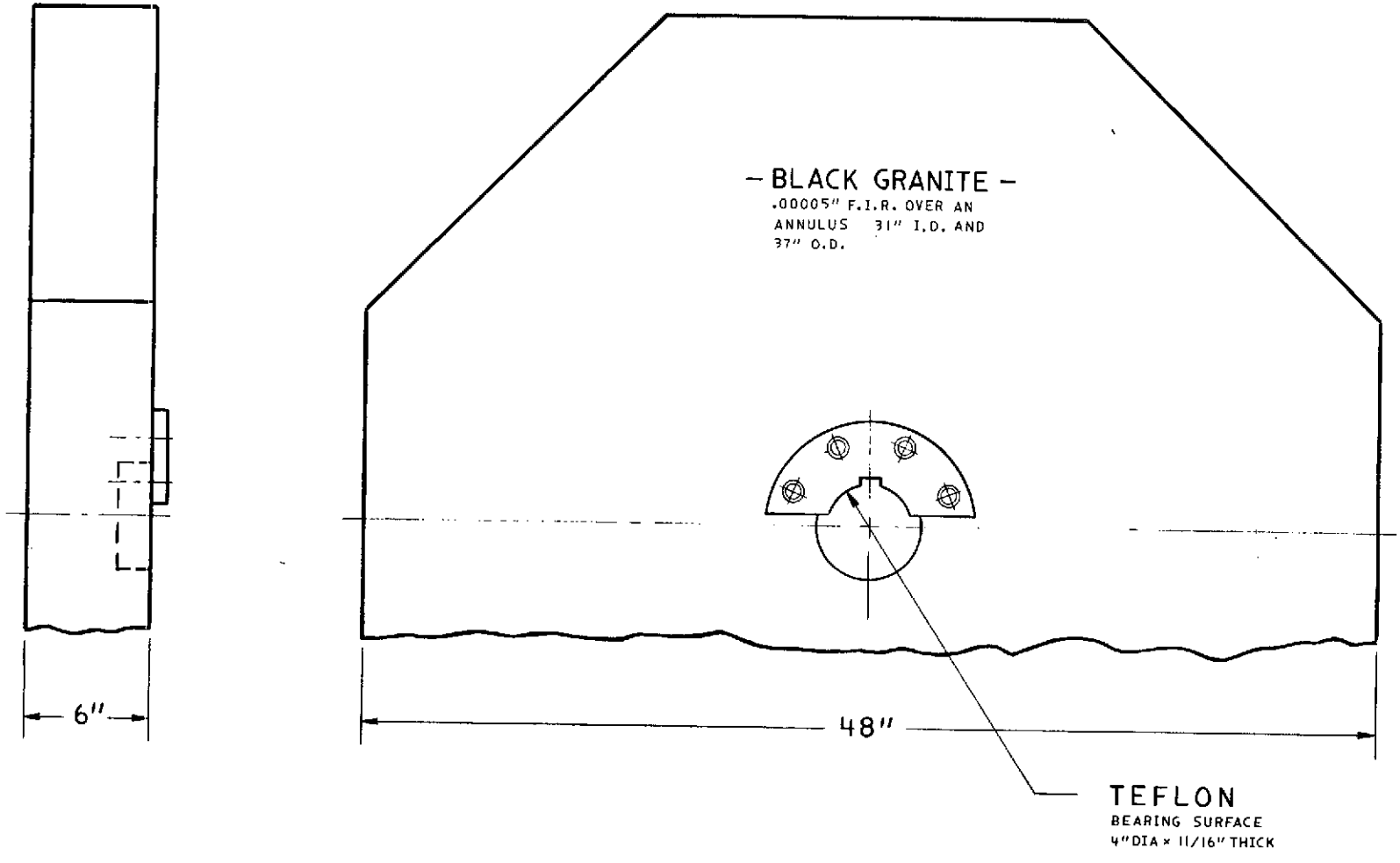

FIGURE 5

ROTOR AND AXLE

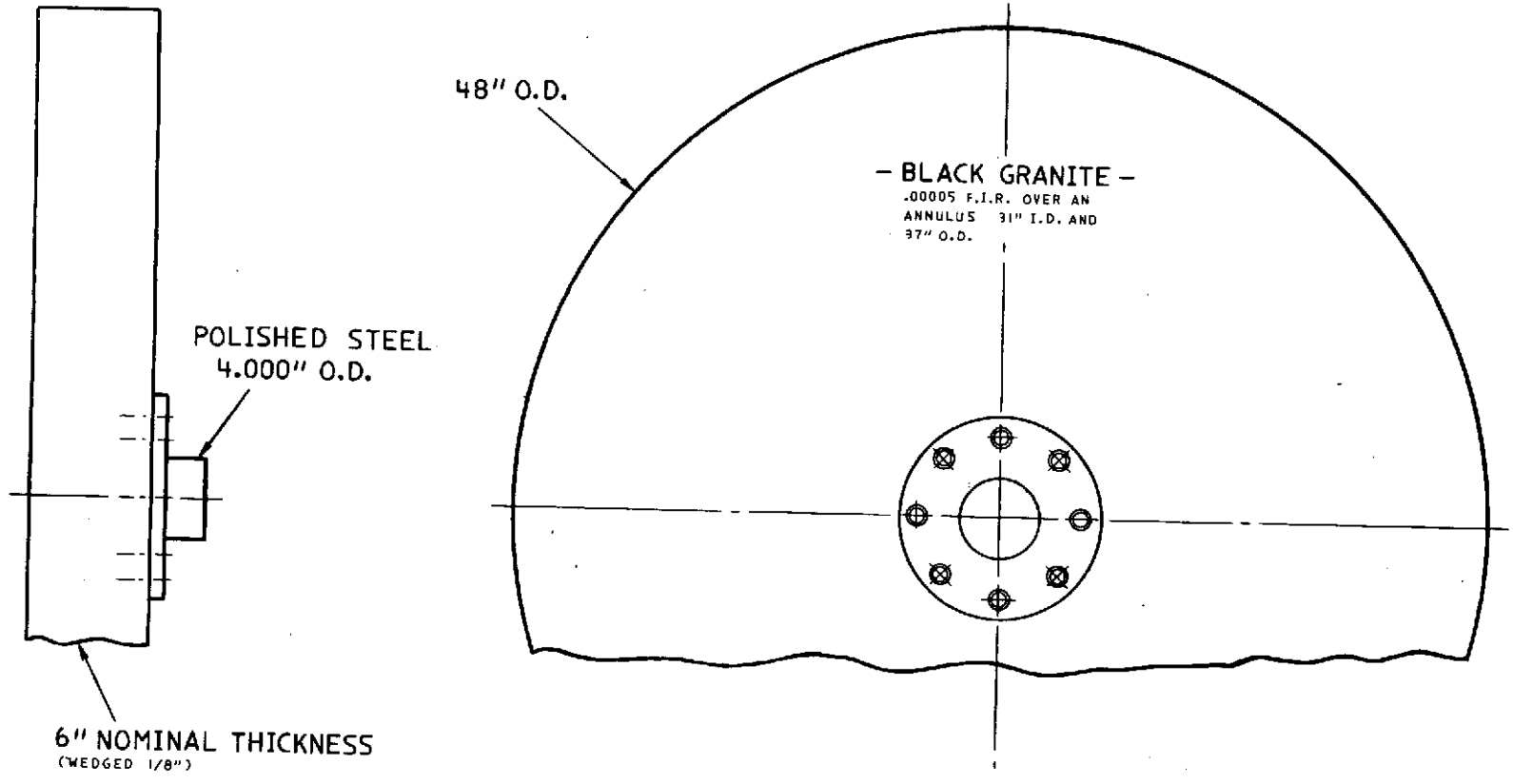

FIGURE 6

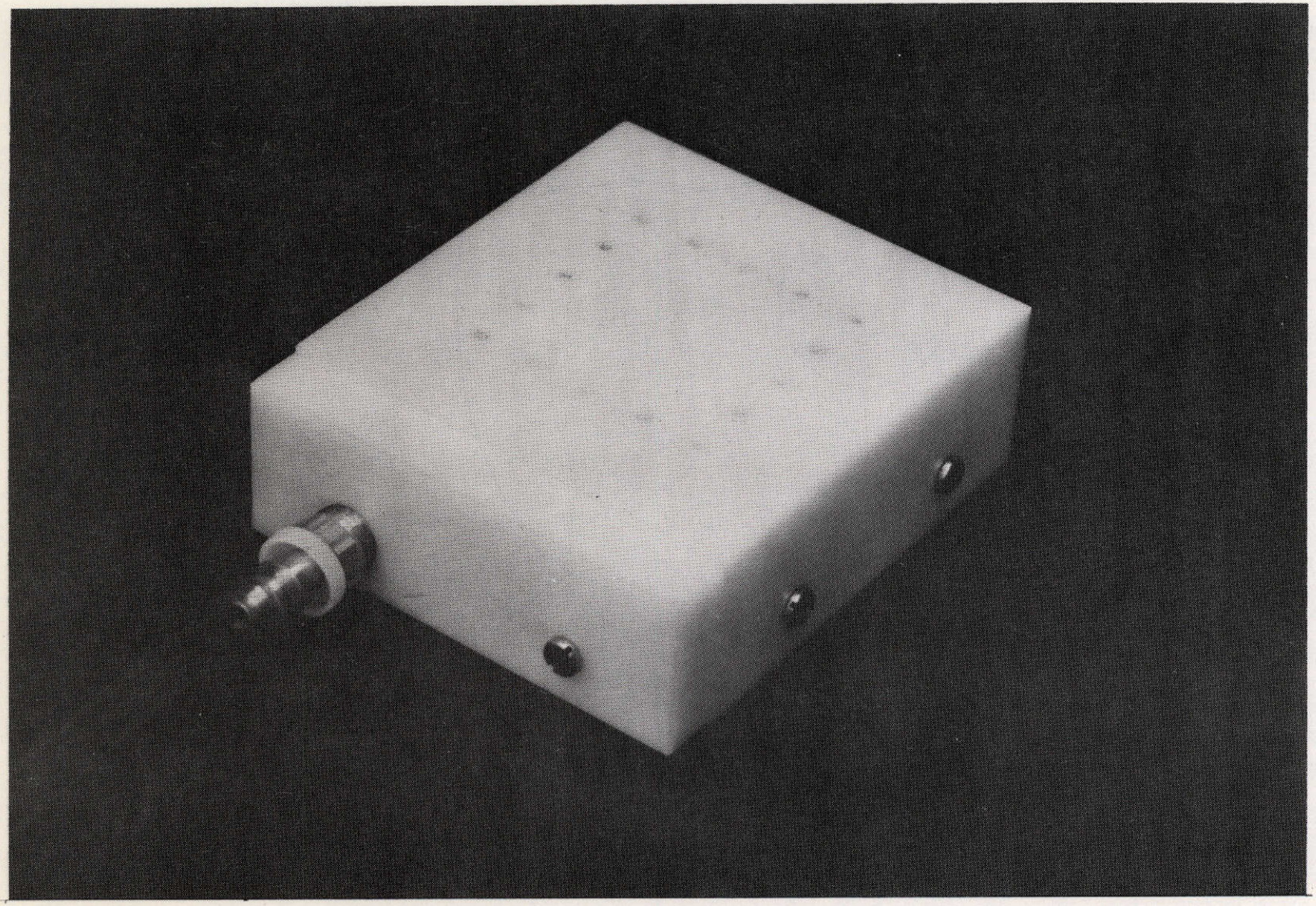

FIGURE 7 AIR BEARING MODULE

MODULE DESIGN

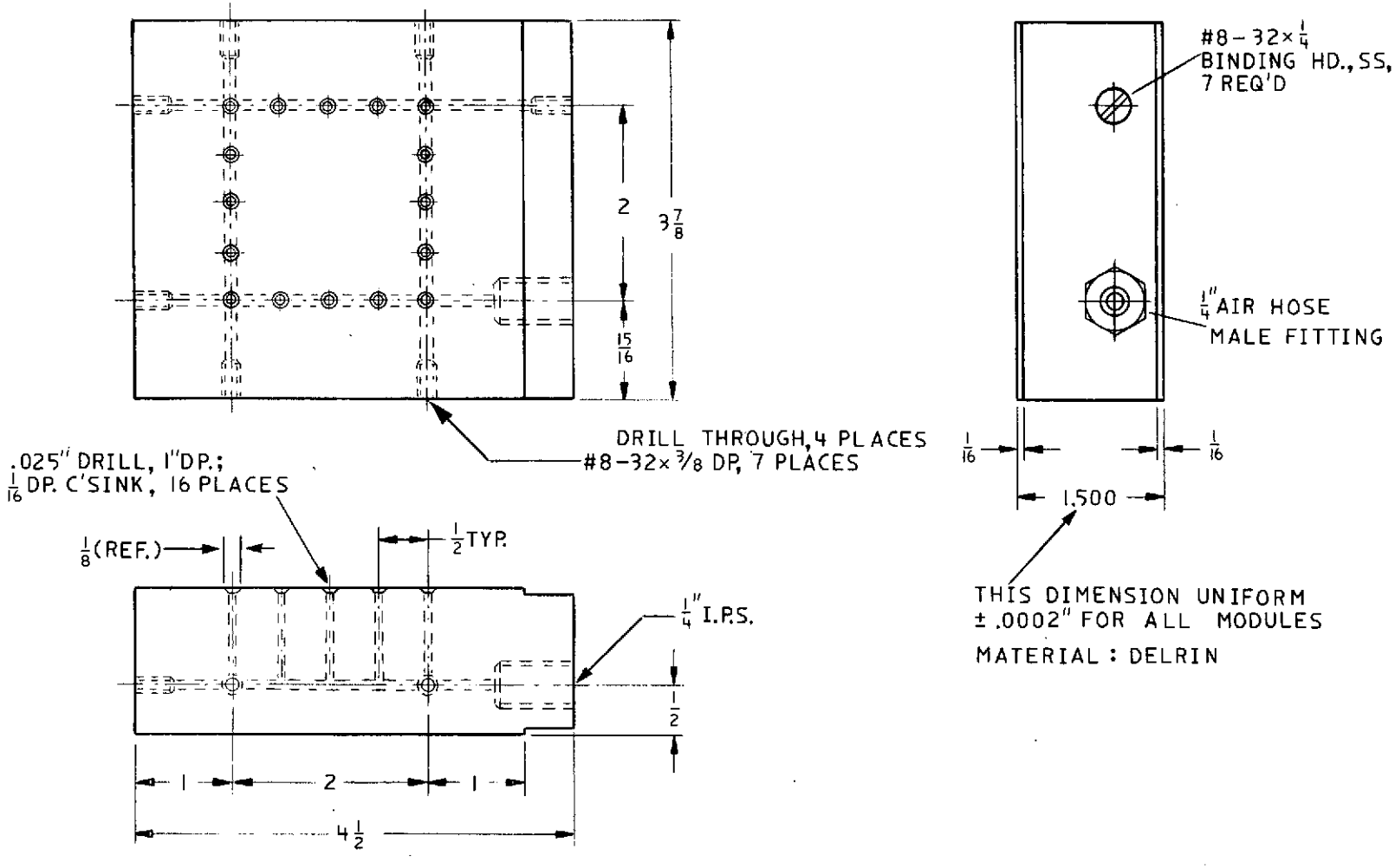

FIGURE 8

3.1.5 Rotary Drive

The rotor is driven from a variable speed DC motor via a pneumatic drive wheel in contact with the rim of the rotor (Figs. 4 & 9). Contact force is maintained at about 5 lbs. by spring loading. Rotary speed is sensed photoelectrically from a divided scale around the rim of the rotor. The speed is displayed digitally and is updated once per revolution. Speed control is open loop.

3.2 Carriage Support Frame

The carriage support frame is shown in Figures 4, 9 and 10. The basic design can be scaled up to much larger size. It is compatible also with future provisions for variable tilt of the frame to accommodate a curved work surface on the mirror. Tilt would be about an axis passing through a reference sphere at the center of the work surface as illustrated in Fig. 2 .

The frame rests kinematically on three ball-and-cup supports from which it can be lifted to allow installation of the mirror. One ball is free to slide on its axle and one cup is free to slide freely on a plate, thus eliminating overconstraint in the supports.

3.3 Radial Motion

The radial drive was designed to provide a highly controllable motion appropriate for eventual use with interferometric control. Accordingly, smooth response rather than accuracy was the design goal. A second design goal was to avoid tight tolerances in components or in adjustments so that the design could readily be scaled up to much larger dimensions.

The radial drive design is shown in Figures 4, 9, and 13. The carriage rides on two rails of polished steel, one flat, the other roofed at 90° to serve as a guide. Slide bearings of teflon (Fig. 12) provide contact between the carriage and the rails; a closely spaced pair of bearings bracket the roof of the guide rail and a widely spaced pair of bearings contact the flat rail. These bearings, not the drive screws, govern the attitude of the carriage about axes in the plane of motion. For future adaptation to precision interferometric control, roller bearings would replace the slide bearings.

Motion is imparted to the carriage by a pair of drive screws (Fig. 9) of .2" pitch, situated on either side of the carriage. Mechanical coupling of the ball nuts to the carriage is flexible for all degrees of freedom except the following: (a) thrust parallel to the screw axis; (b) twist about the screw axis. Thrust parallel to the screw axis is transmitted through rods (Fig. 11) that are longitudinally stiff but laterally are slightly flexible. Straightness and parallelism of the drive screws thus is not of critical importance. Twist of the ball nuts about the screw axis is prevented by torsion bars (Figs. 9 and 11) coupled to the carriage through leaf springs which likewise accommodate themselves to small deviations from straightness and parallelism in the drive screws.

The attitude of the carriage about an axis normal to the plane of motion is governed by the drive screws, not by the carriage rails. A small amount of yaw in the carriage is of no consequence, hence precision in the pitch of the screws is not critical. Each screw is fitted with an opposing pair of ball nuts tightened against one another to reduce hysteresis.

The two drive screws operate synchronously from a worm driven by a stepper motor (Fig. 9). Each step of the motor advances the carriage 0.5μm. Control is manual. For future adaptation to precision interferometric control, an additional fine motion (e.g., piezoelectric) would be required for the scribing lens in order to subdivide the steps and to compensate for residual hysteresis. Such a fine radial motion is outside the scope of the present investigation.

3.4 Laser Stylus

Light for scribing originates from an argon laser (located in the background of Fig. 4). This laser is capable of emitting a total of 300 milliwatts uniphase, principally in the spectral lines at 488nm and 514nm. A pentaprism on the carriage (Fig. 9) directs the beam downward through a 20X microscope objective which focuses the beam onto the surface of the mirror at a cone angle (between the $1/e^2$ intensity points) of approximately $f/2.3$.

The laser beam is aligned parallel to the translation axis of the carriage so that translation of the carriage does not cause the beam to walk across the scribing lens. This arrangement was possible because the work surface was flat and a variable tilt to the frame was not required in the present investigation. To accommodate a variable tilt in future applications, the laser beam would approach along the axis of tilt and would be directed to the pentaprism via mirrors affixed to the frame.

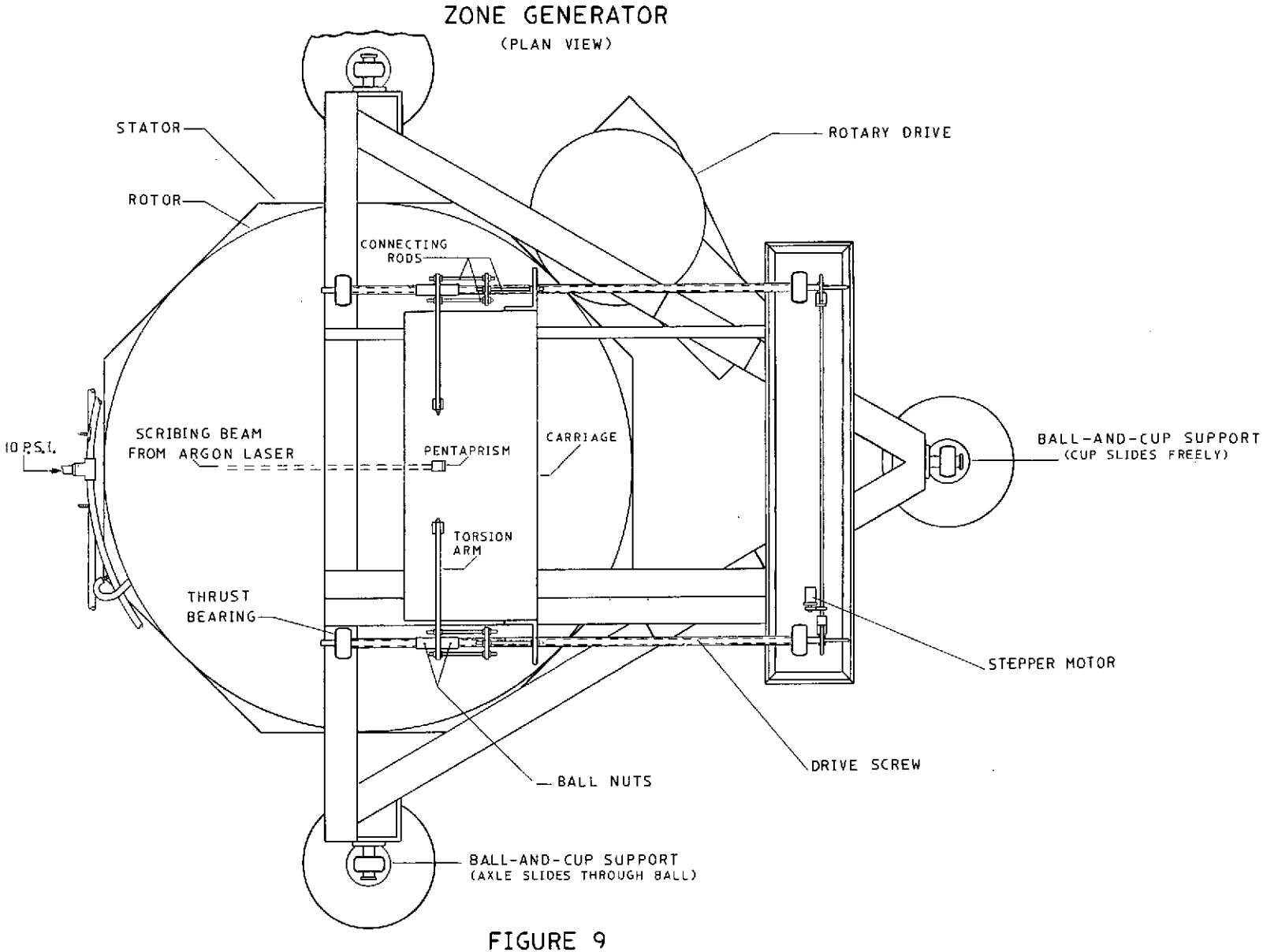
ZONE GENERATOR
(PLAN VIEW)
STATOR
ROTOR
ROTARY DRIVE
CONNECTING RODS
10 P.S.I.
SCRIBING BEAM FROM ARGON LASER
PENTAPRISM
CARRIAGE
BALL-AND-CUP SUPPORT
(CUP SLIDES FREELY)
TORSION ARM
THRUST BEARING
STEPPER MOTOR
DRIVE SCREW
BALL NUTS
BALL-AND-CUP SUPPORT
(AXLE SLIDES THROUGH BALL)

FIGURE 9

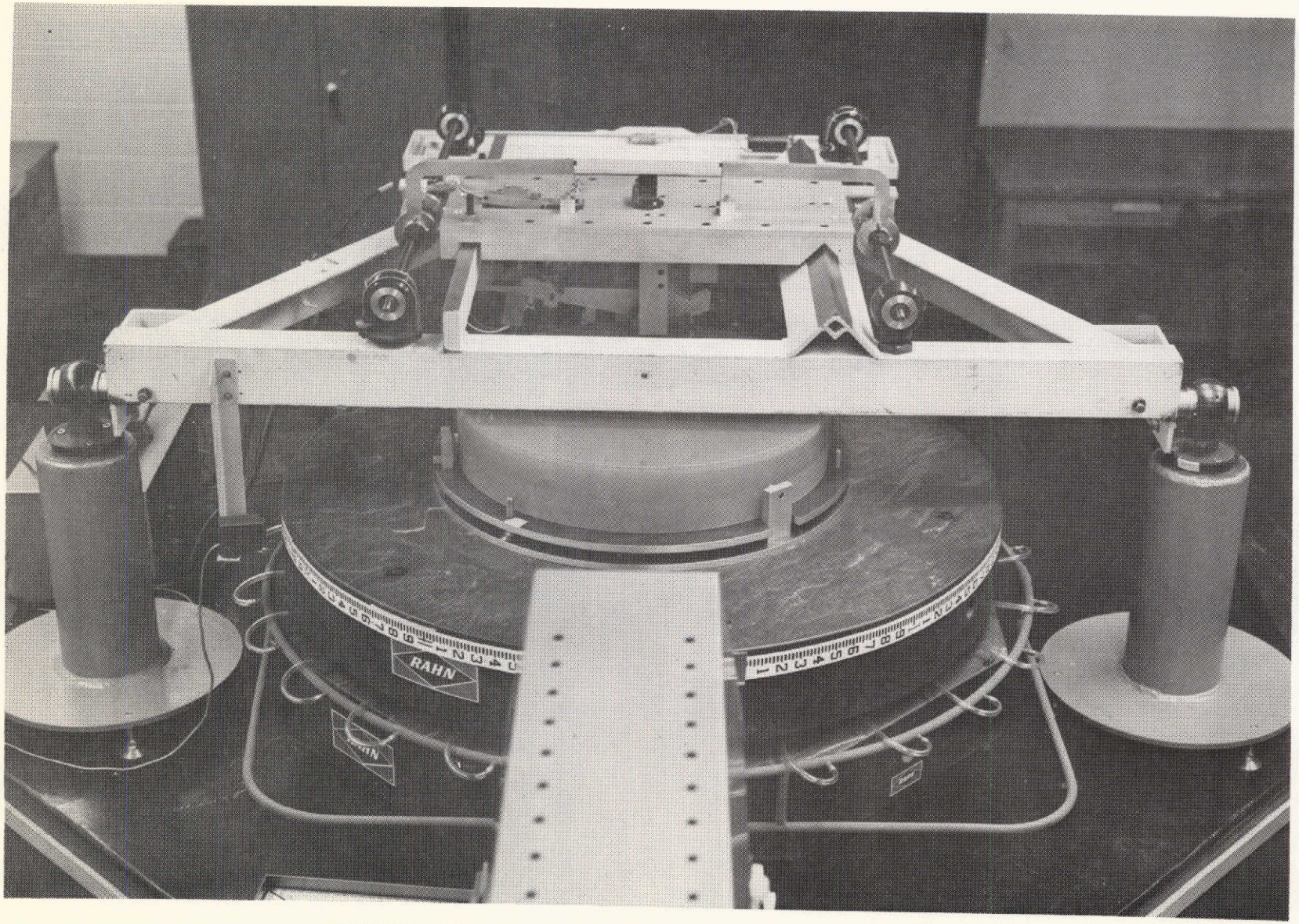

FIGURE 10 TURNTABLE AND CARRIAGE

FIGURE II CARRIAGE DRIVE

3.5 Mirror

The focus control operates off of a Cer-Vit® mirror 60 cm in diameter. At this diameter a linear speed exceeding 1 m/sec can be attained. This linear speed is considered realistic for eventual use with mirrors of much larger diameter. The mirror is flat to ± 2 μm. Tilt relative to the axis of rotation is adjustable.

3.6 Focus Control

Closed loop focus control is provided by the system shown in Figures 12, 13 & 14. In this system the focal position of the scribing lens is controlled by pivot action of the focus control arm on which the scribing lens is mounted. The scribing lens is laterally offset from the pivot axis by 0.5 inch. The pivot bearings are steel pins forced into "V"-notches by gravity and spring pressure. The pivot axis runs in the radial direction so that the focal motion will not cross-couple with the radial motion even if the pivot axis and the nodal point of the scribing lens are not at exactly the same elevation.

A stepper motor actuates the focus control arm. The shaft of the stepper motor is threaded through a plate affixed to the carriage. Contact between the end of the motor shaft and the focus control arm is maintained by spring pressure. The stepper motor advances along a pair of precision guides by 10 micrometers/step. The resultant rotation of the focus control arm advances the scribing lens by 0.5 μm/step.

Changes in the focal position of the scribing lens with respect to the work surface are sensed directly by an optical system mounted on the focus control arm (Fig. 14). The light source for this system is a 1 milliwatt He-Ne laser which, because of its mass, is not mounted on the focus control arm but is affixed directly to the carriage. The He-Ne laser beam is brought to an astigmatic focus on the work surface in a horizontal line image about 1 mm long centered on the focal point of the "laser stylus". A concave mirror reimages this line image back upon itself. From there it is reimaged onto a "knife edge" which divides the aperture into a reflective half and a transmissive half.

That portion of the final image which impinges upon the reflective side of the "knife edge" (Fig. 15) is reflected downward to a silicon photodiode. The other portion of the image which impinges upon the transmissive side of the "knife edge" continues onward to a second photodiode. These two photodiodes operate in a push-pull arrangement so as to provide a null signal when the image is divided into approximately equal parts by the "knife edge".

CARRIAGE AND FOCUS CONTROL ASSEMBLIES

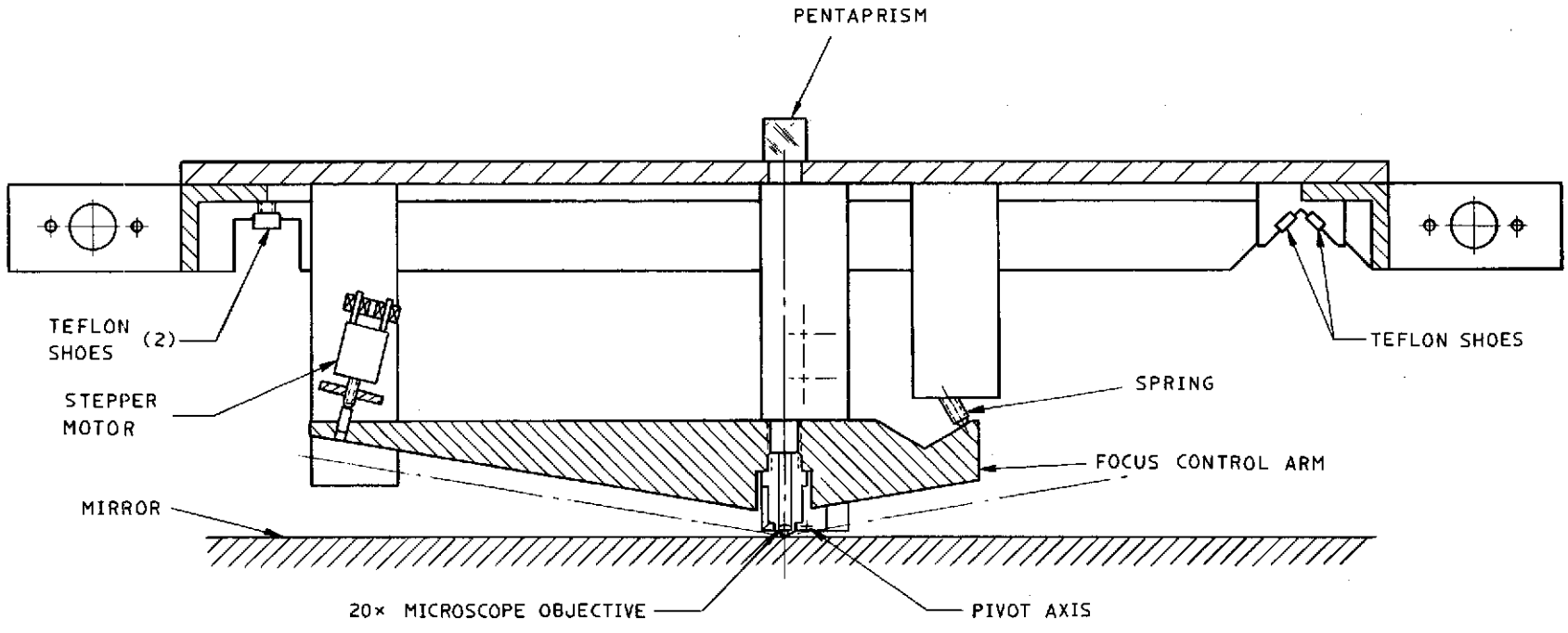

FIGURE 12

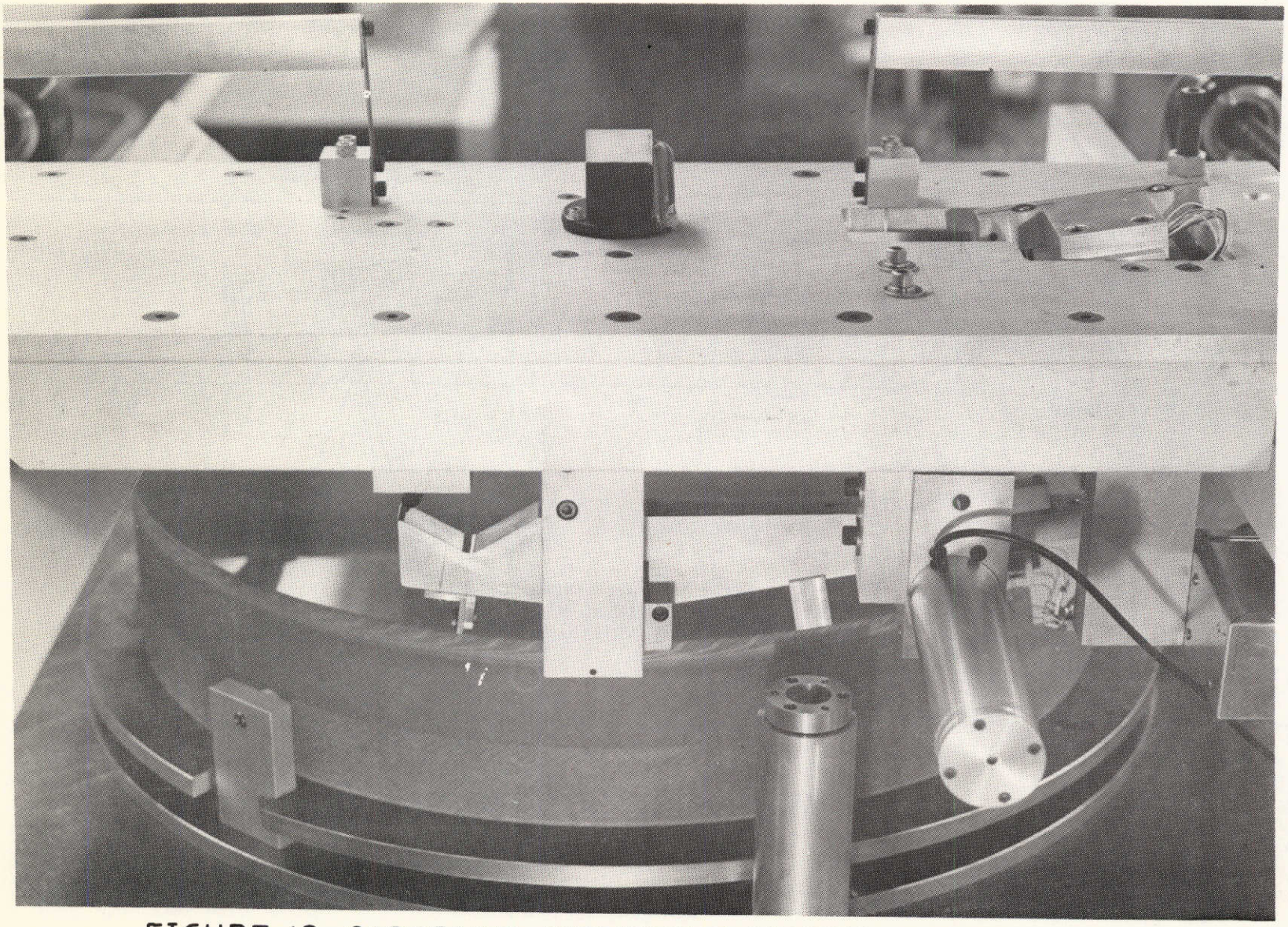

FIGURE 13 CARRIAGE AND FOCUS CONTROL ARM

FOCUS SENSOR ASSEMBLY

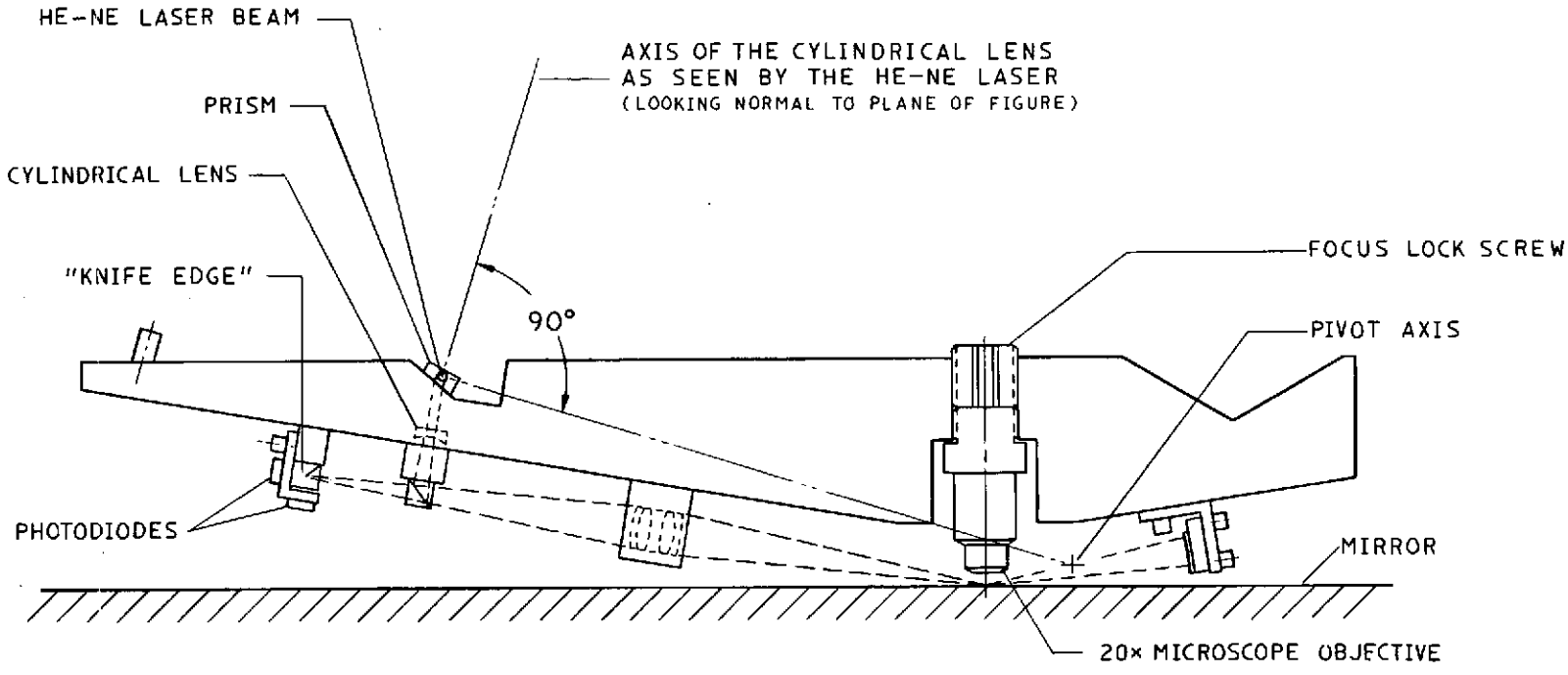

FIGURE 14

FOCUS CONTROL SCHEMATIC

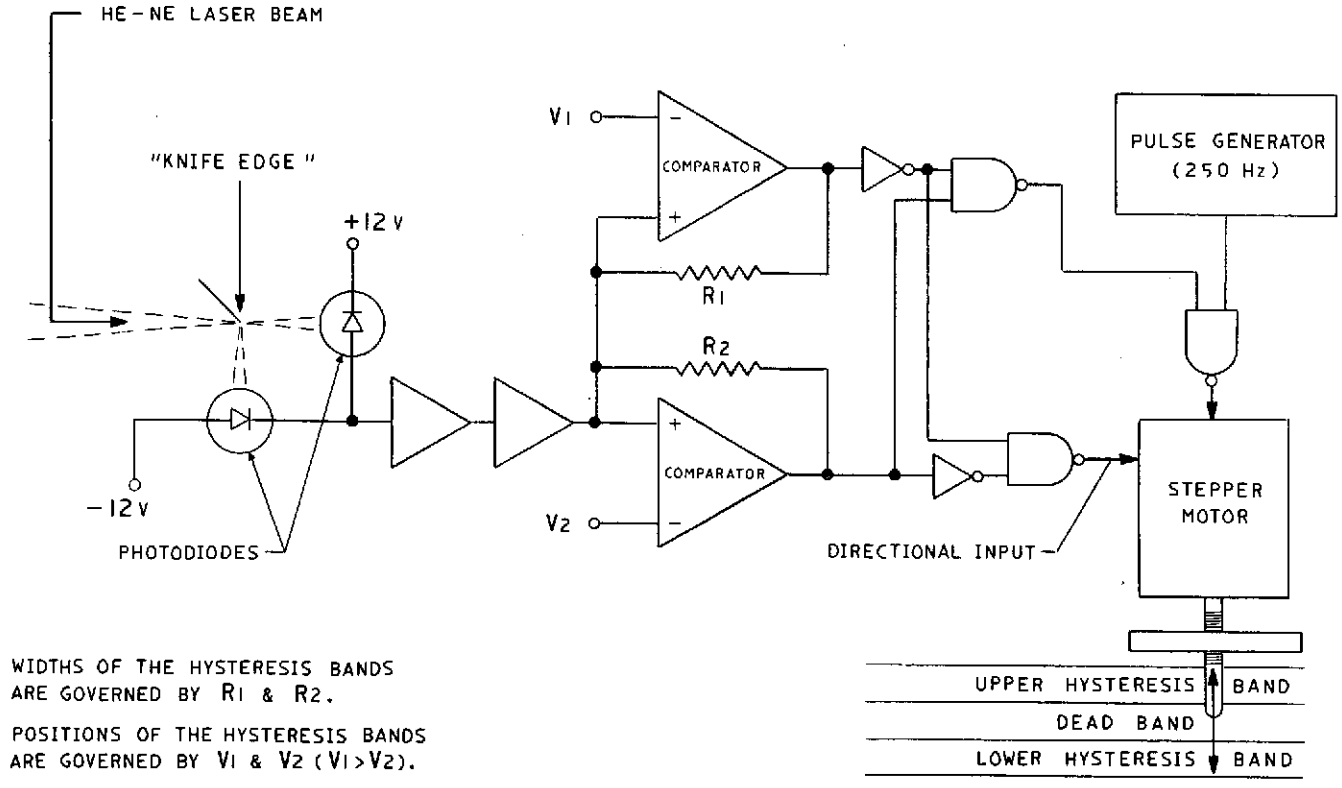

WIDTHS OF THE HYSTERESIS BANDS ARE GOVERNED BY R1 & R2.

POSITIONS OF THE HYSTERESIS BANDS ARE GOVERNED BY V1 & V2 (V1>V2).

FIGURE 15

The focus sensor is designed to be insensitive to tilt of the work surface so that the design is applicable to concave or convex work surfaces. This insensitivity results from the fact that the work surface is double-passed in a manner that makes the astigmatic focus at the "knife edge" invariant to tilt of the work surface. For small displacements, the system is also insensitive to lateral walk of the He-Ne beam across the cylindrical lens. This is due to the circumstance that the direction of walk is parallel to the astigmatic axis of the cylindrical lens and to the circumstance that double reflection of the beam from the work surface maintains symmetry on the work surface.

Error signals from the sensor actuate the focus control motor in a closed loop as indicated in Fig. 15 . Pulses to the stepper motor originate from a 250Hz oscillator. These pulses are gated according to the level of the error signal. As indicated in Fig. 15 , provision is made for a dead band bracketed by control regions, each with its own hysteresis band.

Adjustment of the focus control is done by adjusting the scribing lens to its proper focal position while the control loop stabilizes the focus control arm. The proper focal position of the scribing lens is that which causes the scribing beam (as observed on a screen at the argon laser) to be exactly retrodirected upon itself by reflection from the work surface.

4. PERFORMANCE

4.1 Rotary Motion

The air bearing was entirely satisfactory. The air gap was 28μm at a pressure of 10 psi. At this pressure, an interferometric test showed no flutter. The lateral bearing, too, was entirely satisfactory. Operation was smooth at rotary speeds up to 1 rev/sec (twice the design goal). Counterbalance for the taper of the rotor (Fig. 6) was not needed. Rotary speed was controllable to better than 1%.

4.2 Radial Motion

The radial motion proved entirely satisfactory for purposes of the present investigation. Alignment of the drive screws parallel to the rails to within .5mm easily sufficed to meet the loose alignment requirements of the design (see Section 3.3). The carriage responded to drive increments as small as 1μm despite friction of the slide. Hysteresis from friction of the slide was 12μm.

4.3 Focus Control

The sensitivity of the focus control is very good. After two reflections from an uncoated work surface, the total light signal at the detectors is 14μ watts. A 25μm displacement of the work surface is sufficient to throw this signal almost entirely onto one detector. Electrical noise is, therefore, no problem in sensing displacements as small as .5μm. Instability in the electrical gain likewise is no problem.

The one serious problem encountered is that reaction from the stepper motor causes hunting when the dead band and the hysteresis bands are setat 1 step (.5μm) each. To prevent hunting, an "A"-frame stiffener was added to the main frame and the dead band and the hysteresis bands were increased to two steps (1μm) each. The focus control then tracked the mirror surface at a linear speed of 1m/sec. (rotary speed, 33 r.p.m.) with the mirror tilted out of the plane of rotation by 15 arc seconds.

5.0 SCRIBING EXPERIMENTS

5.1 The turntable and "laser stylus" were used to scribe lines in various coatings on a "Cer-Vit" substrate. The samples used were small enough to be accommodated by an electron microscope. The focus control could not be used on these small samples. The sample surface was therefore tilted slightly in the tangential direction so as to cause the surface to pass through the region of sharpest focus of the scribing beam.

5.2 Scribing speeds were typically of the order of 1.5m/sec as this was considered to be a practical speed for eventual use with very large mirrors. At these speeds, the .3 watt maximum power of the scribing beam exceed actual requirements in all cases.

5.3 The principal objective of these experiments was to scribe zones of Type B (see Fig. 3). Ideally, Type B zones have a "square wave" profile with a step height of $\frac{\lambda_o}{4}$, where λ_o denotes the wavelength of the laser light used in the telescope monitor. Zone widths vary inversely with the zone radius and inversely with the aperture ratio of the mirror (see Ref. (1) on p. 1). In the present experiments, λ_o was taken as 632nm in which case the ideal step height is 158nm. Zone widths of interest covered the range from 1.5μm to 10μm.

5.4 In principle, the final zone profile may consist either of narrow grooves in a coating $\frac{\lambda_o}{4}$ thick or of narrow ridges $\frac{\lambda_o}{4}$ high on the mirror substrate itself. The latter is preferable since in this case the uniformity of the step height does not materially affect the quality of the mirror. The experimental effort was, therefore, directed toward a three-step process in which the first step was to scribe sharp lines through a masking layer; the second step was to deposit a $\frac{\lambda_o}{4}$ overcoat, and the third step was to remove the masking layer and with it the $\frac{\lambda_o}{4}$ overcoat except where it adhered to the substrate within the lines ruled through the masking layer.

5.5 Initial experiments were conducted with base layers which do not require vacuum deposition. The first of these experiments was with a layer of halowax, applied by whirling and dyed to give absorption of blue light. This proved unsuitable because the scribed lines were too broad and a residue within the lines prevented adhesion of the overcoat to the substrate. In further experimentation with whirled coatings, a base layer of photosensitive

gelatin was applied, then hardened by exposure to U.V. and dyed to give absorption to blue light. In this case, the "scribed" lines did not evaporate but instead were hardened further by the laser light, producing raised rather than lowered zones after development. Resolution was poor, the narrowest line being 5μm wide.

5.6 Subsequent experiments were conducted using coatings deposited by evaporation in a vacuum. In the first set of these experiments, zinc was used as the masking layer. Zinc was chosen because its melting point (419°C) and its evaporation point (907°C) are relatively close together. It was therefore hoped that evaporation would be clean without the problem of droplet formation which occurs in lines scribed with laser beams in bismuth, cadmium, gold, cobalt, and zirconium (see "Continuous Wave Laser Recording in Metallic Thin Films" by A.L. Harris; M. Chen; H.L. Bernstein; Image Technology, April/May, 1970).

5.7 Initial results with thin masking layers of zinc (of the order of 15nm thick) were encouraging; sharp lines as narrow as 2.6μm were scribed with no serious problem with droplets (see Fig. 16). Adherence of a chrome overcoat within the scribed lines was good provided the chrome layer was sufficiently thin (e.g. 15 nm). However, when the zinc masking layer was etched from under the chrome with sodium hydroxide, the chrome fractured irregularly along the edges of the scribed lines. When the thickness of the chrome overcoat was increased to $\frac{\lambda_o}{4}$, the chrome parted from the Cer-Vit substrate instead of fracturing at the edges of the lines. A $\frac{\lambda_o}{4}$ overcoat of Si 0_2 was used instead of chrome. It then proved difficult to etch away the zinc from beneath the protective overcoat of Si 0_2. Heating to 350°C sublimed the zinc but vigorous cleaning was needed to remove the overhanging Si 0_2 and the resulting lines were ragged.

5.8 To produce clean fracture of the $\frac{\lambda_o}{4}$ overcoat at the edges of the scribed lines, it appeared highly desirable that the depth of the scribed line equal or exceed $\frac{\lambda_o}{4}$ and that the sides of the scribed line be steep. Experiments to generate such profiles were undertaken using much thicker masking layers than before. The first attempt was made with a masking layer of Magnesium Fluoride (MgF_2) having a thickness of $\frac{\lambda_o}{4}$. In order to transfer heat to the transparent MgF_2 layer, it was overcoated with an absorptive layer of zinc

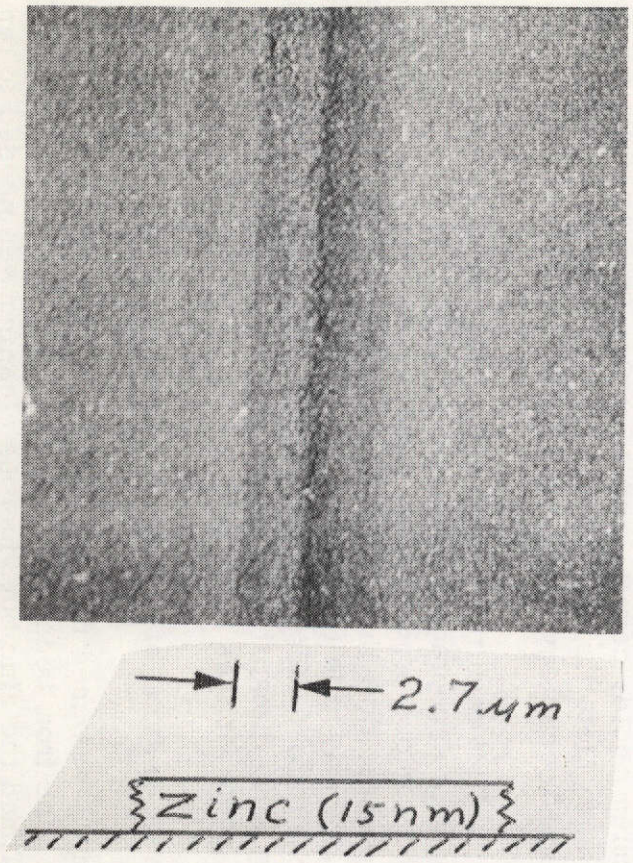

FIGURE 16 ZINC

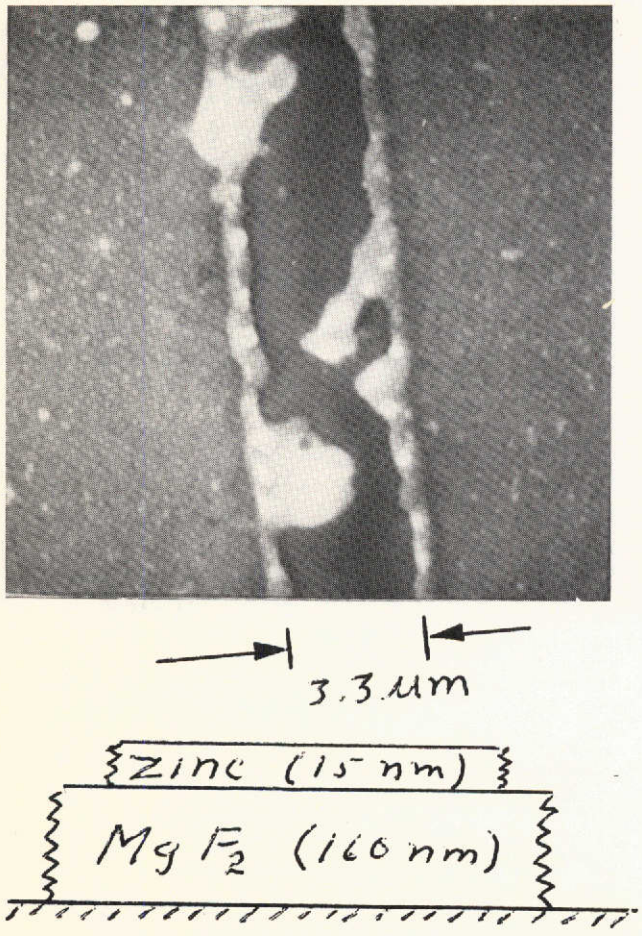

MAGNESIUM FLUORIDE
UNDER ZINC
FIGURE 17

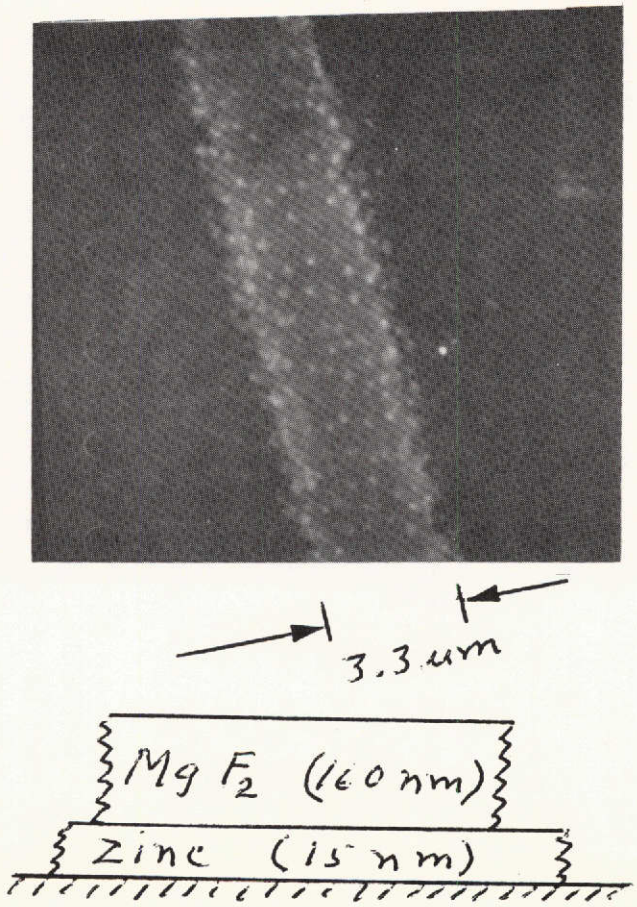

MAGNESIUM FLUORIDE
OVER ZINC
FIGURE 18

32nm thick. Heat transfer was effected and a narrow line was generated (Fig. 17), but irregular melting of the MgF_2 produced ragged edges to the line. Further experiment with the zinc layer under the MgF_2 left many small droplets within the scribed line (Fig. 18).

5.9 In order to avoid droplets and other irregularities which melting produces, experiments were undertaken using selenium as the masking layer. Selenium was chosen because the absorption characteristics of a $\frac{\lambda_o}{4}$ layer of selenium are almost ideal for argon light (see spectrophotometer results in Fig. 19). The radiant energy penetrates well into the layer and is almost totally absorbed. Furthermore, the evaporation temperature (688°C @ 1 atm) is low enough to permit high-speed scribing but the vapor pressure (10^{-6} torr @ 125°C) is low enough that selenium can be deposited in a vacuum. Selenium, however, is toxic and must be handled with caution.

5.10 Initial results with selenium looked very promising. Smooth, narrow lines were easily scribed through masking layers $\frac{\lambda_o}{4}$ thick. No droplets were evident. A chrome overcoat was applied and the selenium mask was removed by heating the sample to 217°C in a vacuum. At this temperature the selenium melted, breaking up the chrome overcoat except where it adhered to the substrate within the scribed lines (Fig. 20). In one instance (Fig. 21) the chrome simply curled away from the edges of the scribed line. After cooling, the sample was scrubbed in acetone to remove the debris and to smooth the edges of the chrome lines.

5.11 Initially, the chrome adhered well to the scribed lines but the edges of the lines were ragged unless the chrome overcoat was much thinner than $\frac{\lambda_o}{4}$. When the chrome layer approached a thickness of $\frac{\lambda_o}{4}$, irregular fracture of the chrome gave ragged edges to the lines (Fig. 21). Attempts were made to steepen the sides of the lines so as to weaken or destroy the continuity of the chrome at the edges of the lines. For this purpose an aluminum undercoat $\frac{\lambda_o}{4}$ thick was applied beneath the selenium layer and attempts were made to etch the scribed lines into the aluminum using the selenium layer as a mask. The selenium, however, would not withstand the etchants (NaOH and $NaCO_3$). As an alternative, the selenium layer was overcoated with zinc in the hope that the more volatile selenium might undercut the zinc, either during the scribing process or later during bombardment in a glow discharge. Problems with non-adhesion of the chrome left this matter unresolved.

TRANSMISSION & REFLECTION OF SELENIUM

(160 NM OF SELENIUM ON 10 MM OF CER-VIT®)

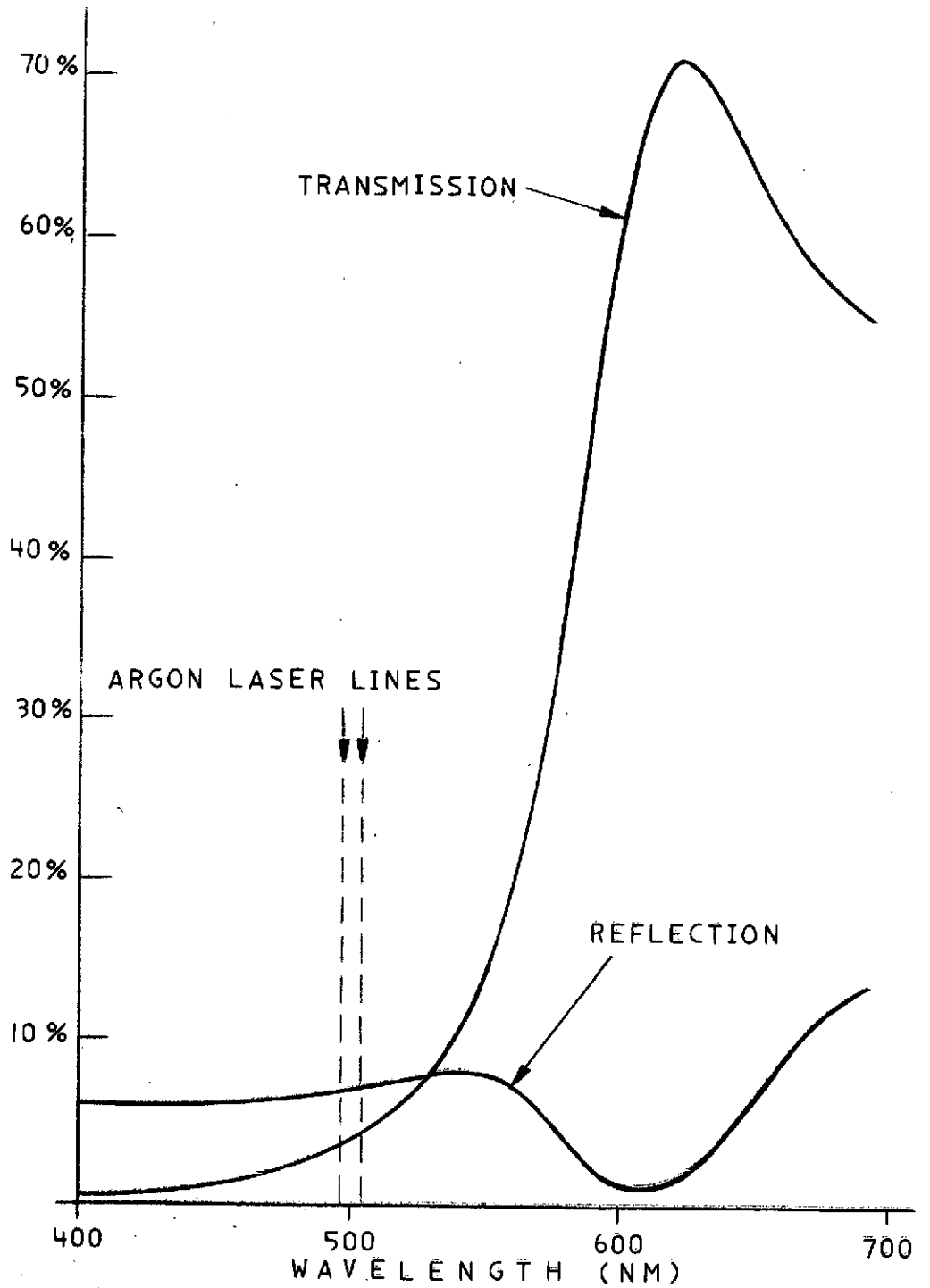

FIGURE 19

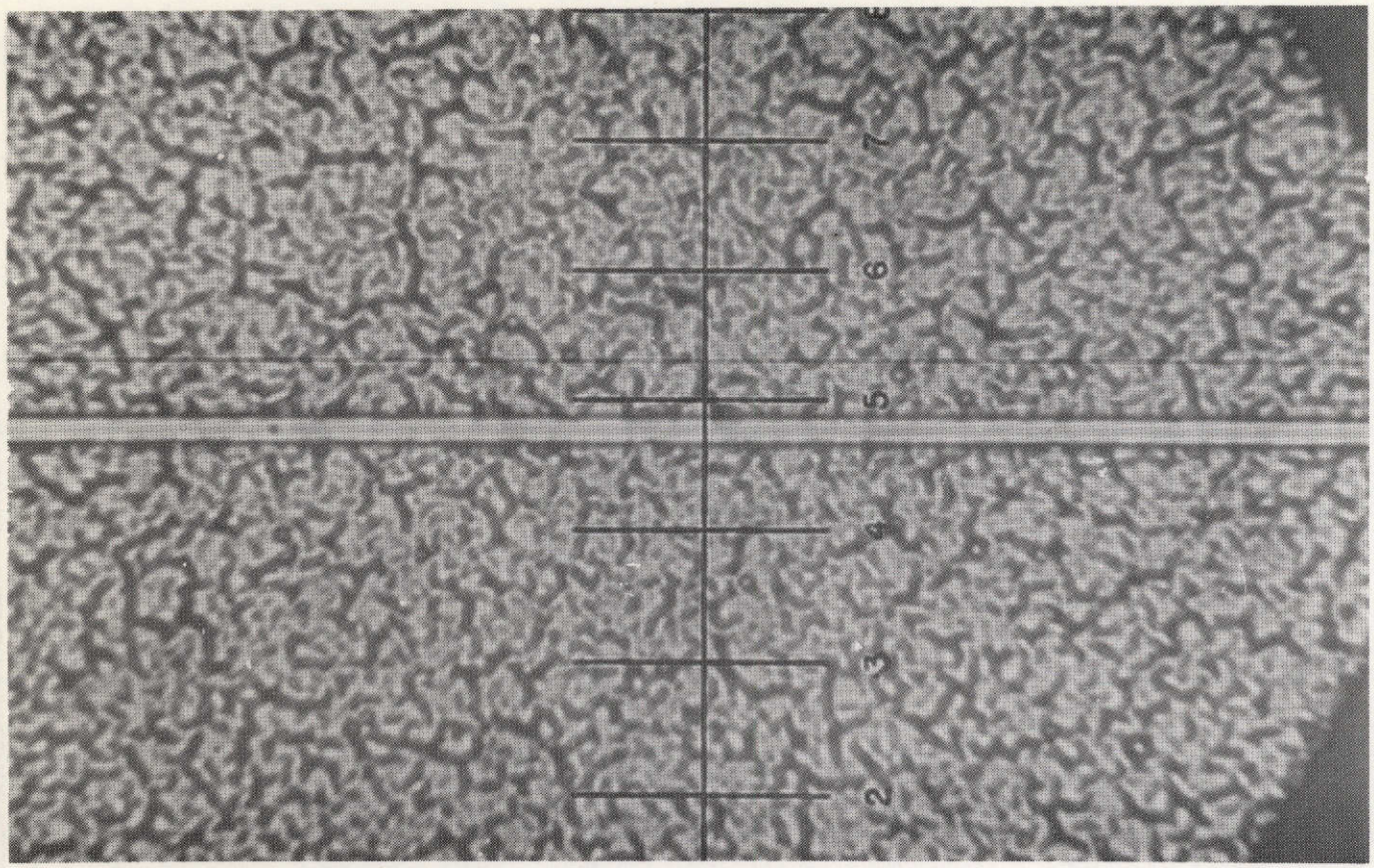

FIGURE 20 _ CHROMIUM ON A SELENIUM MASK — AFTER HEATING MELTING OF THE SELENIUM BREAKS UP THE CHROMIUM EXCEPT WHERE IT ADHERES TO THE SUBSTRATE WITHIN THE SCRIBED LINE

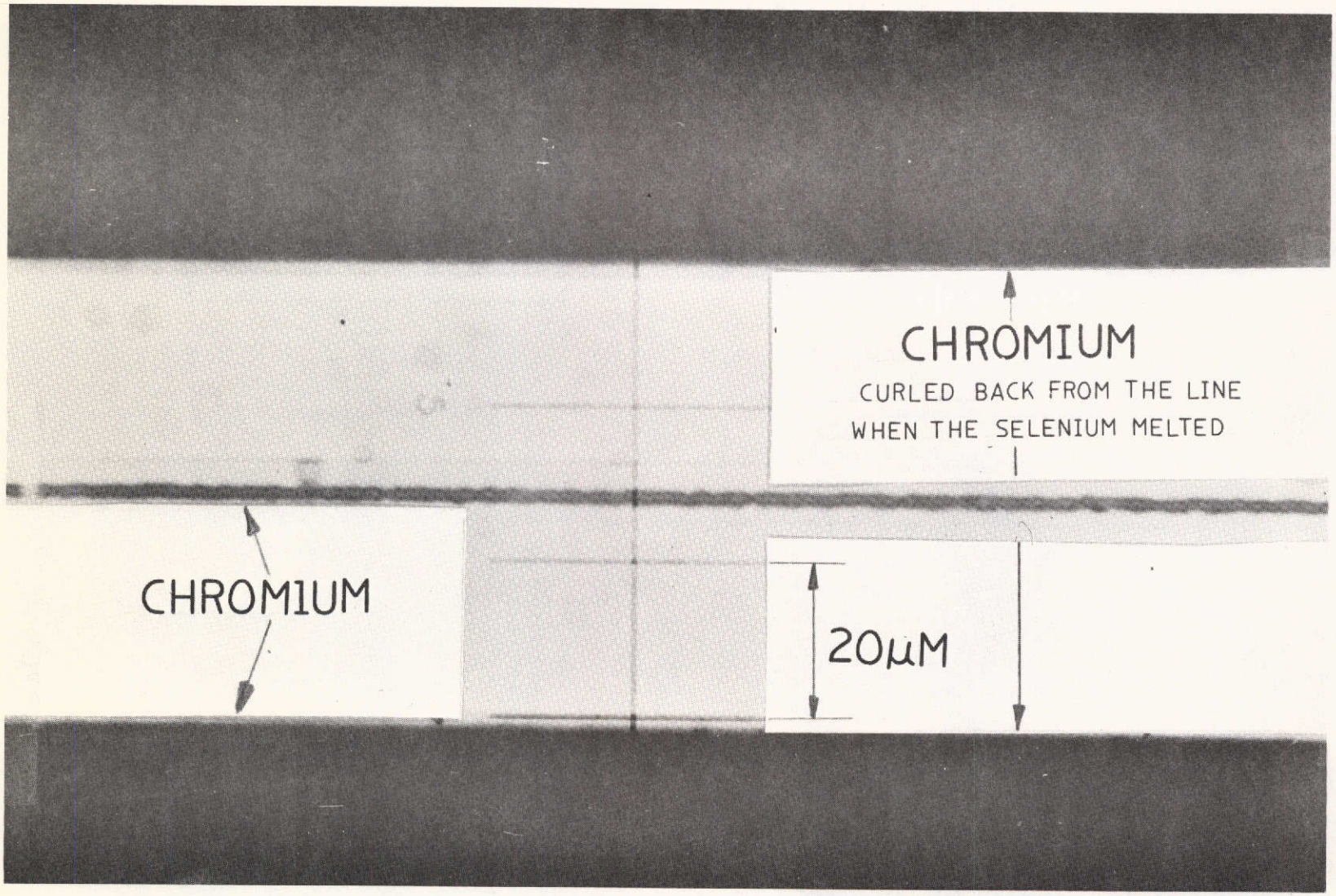

FIGURE 21 CHROMIUM LINE

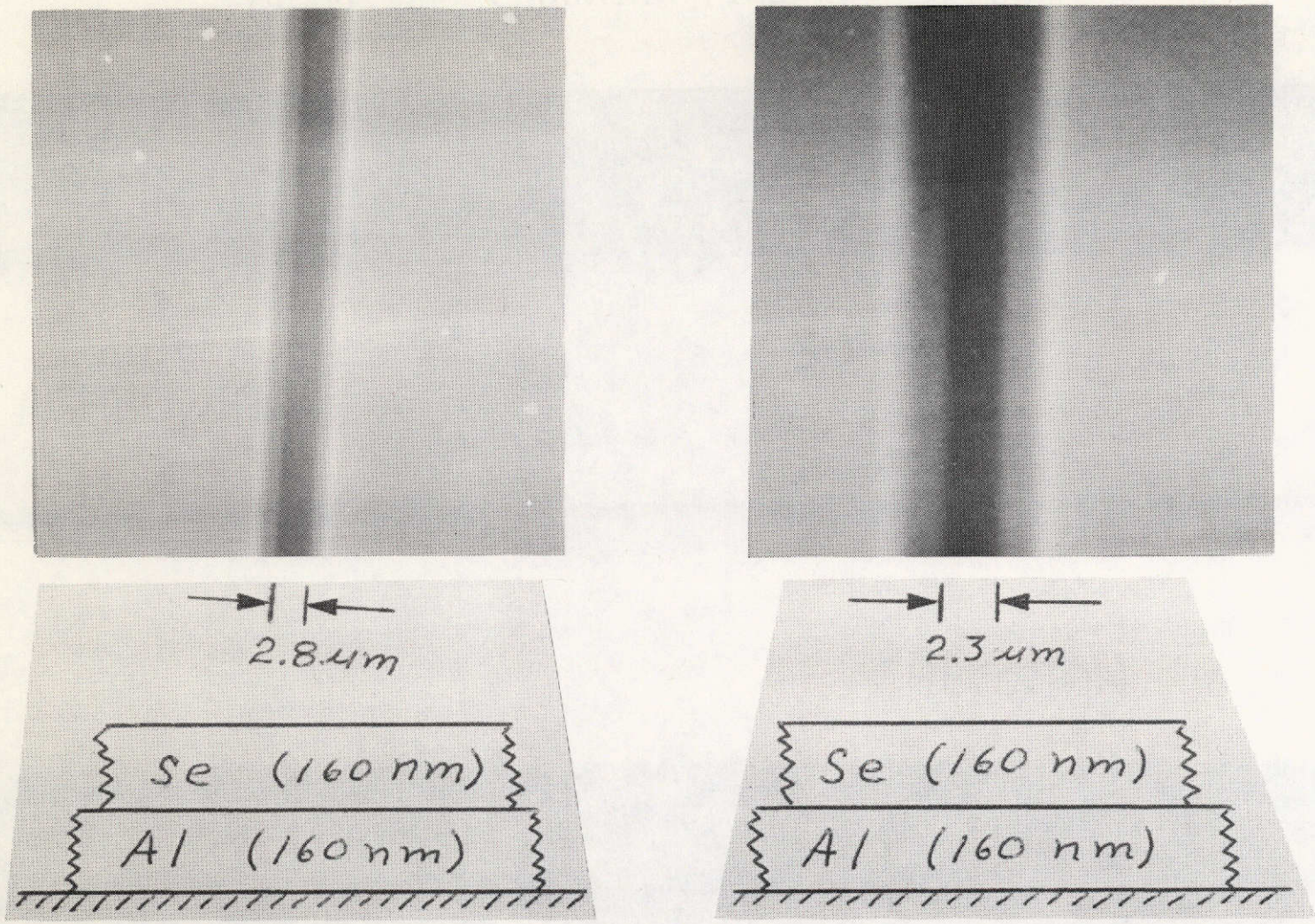

FIGURE 22 SELENIUM ON ALUMINUM

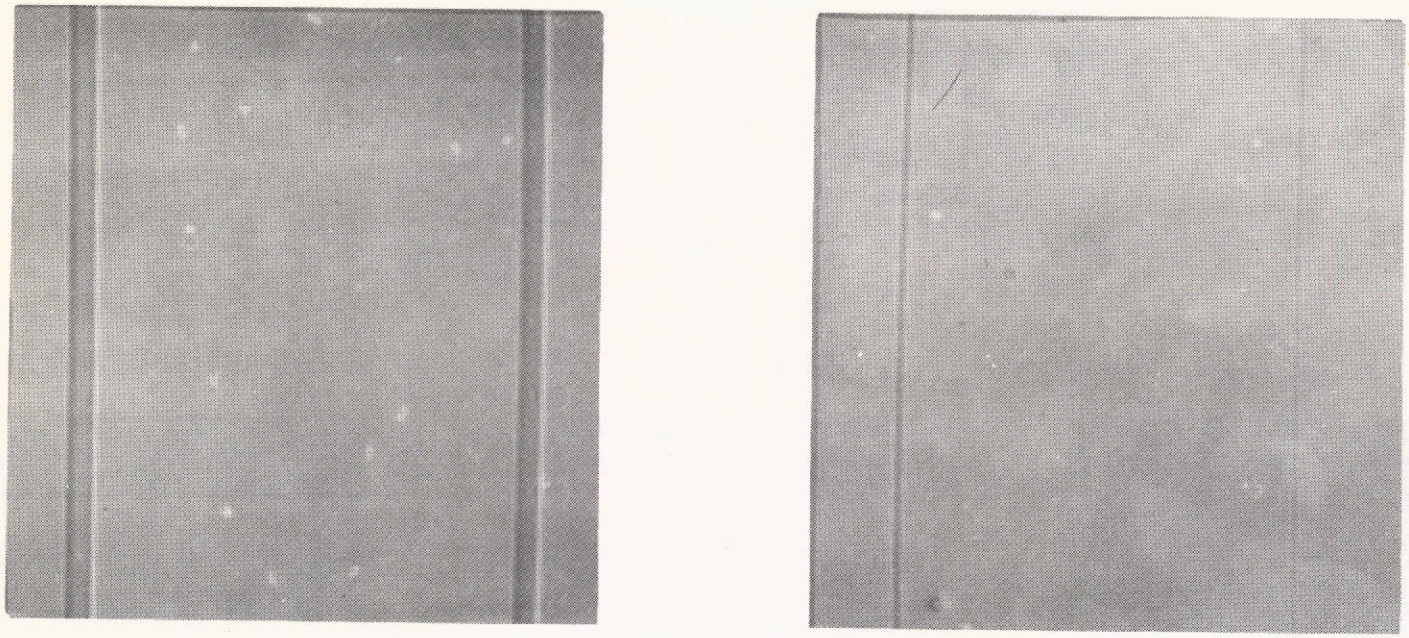

FIGURE 23 SELENIUM ON CHROMIUM (315x)

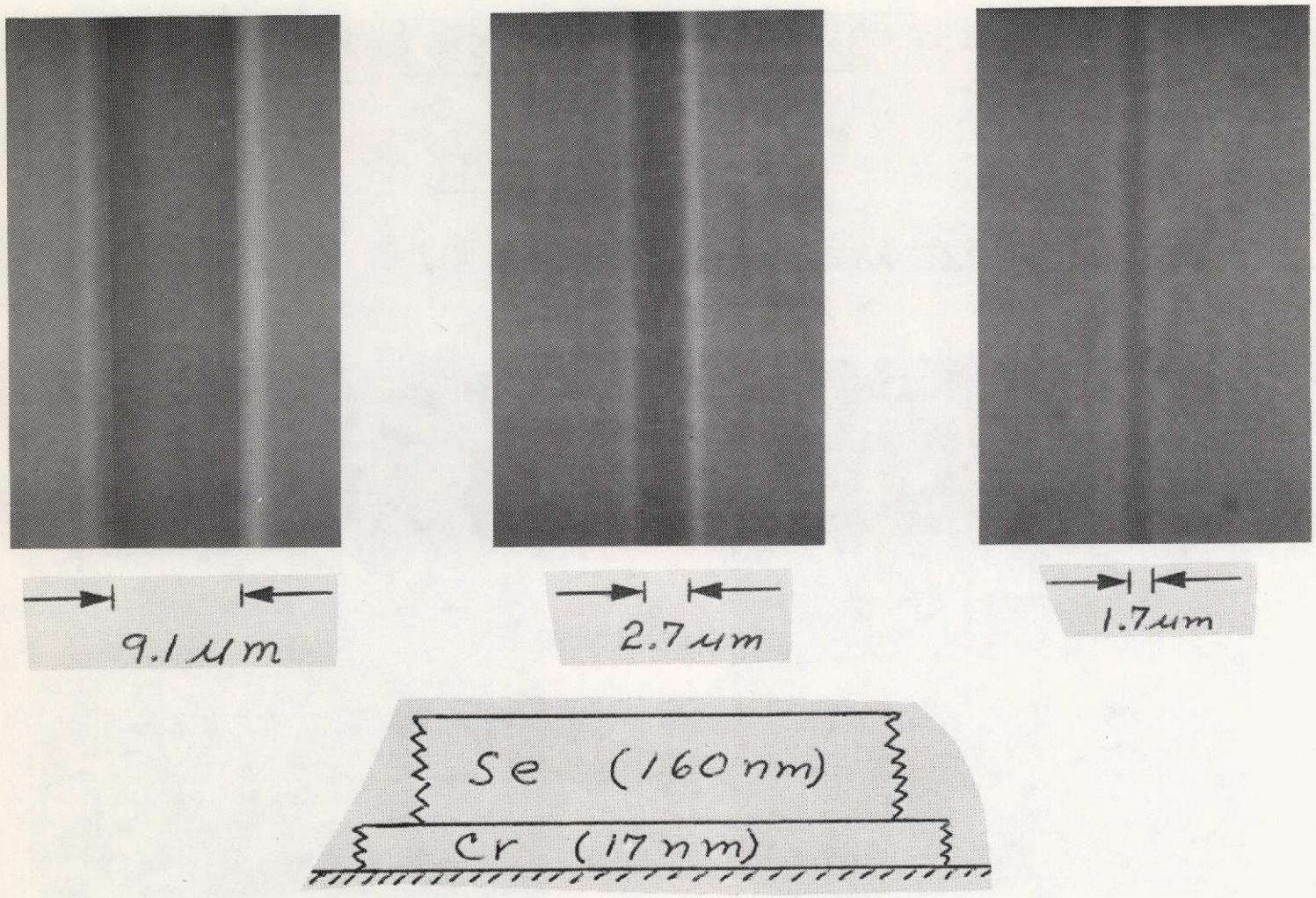

FIGURE 24 SELENIUM ON CHROMIUM (2100 X)

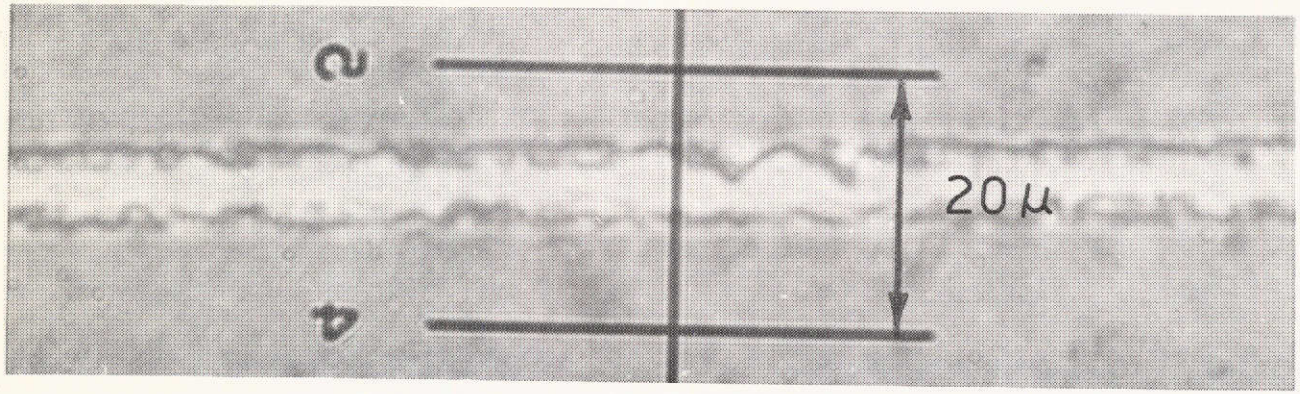

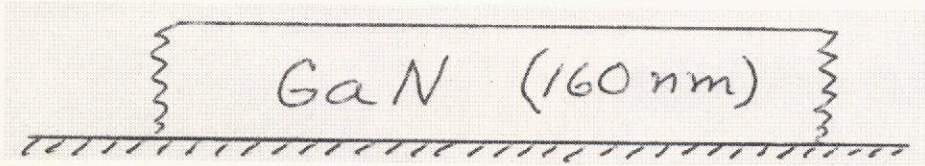

FIGURE 25 GALLIUM NITRIDE

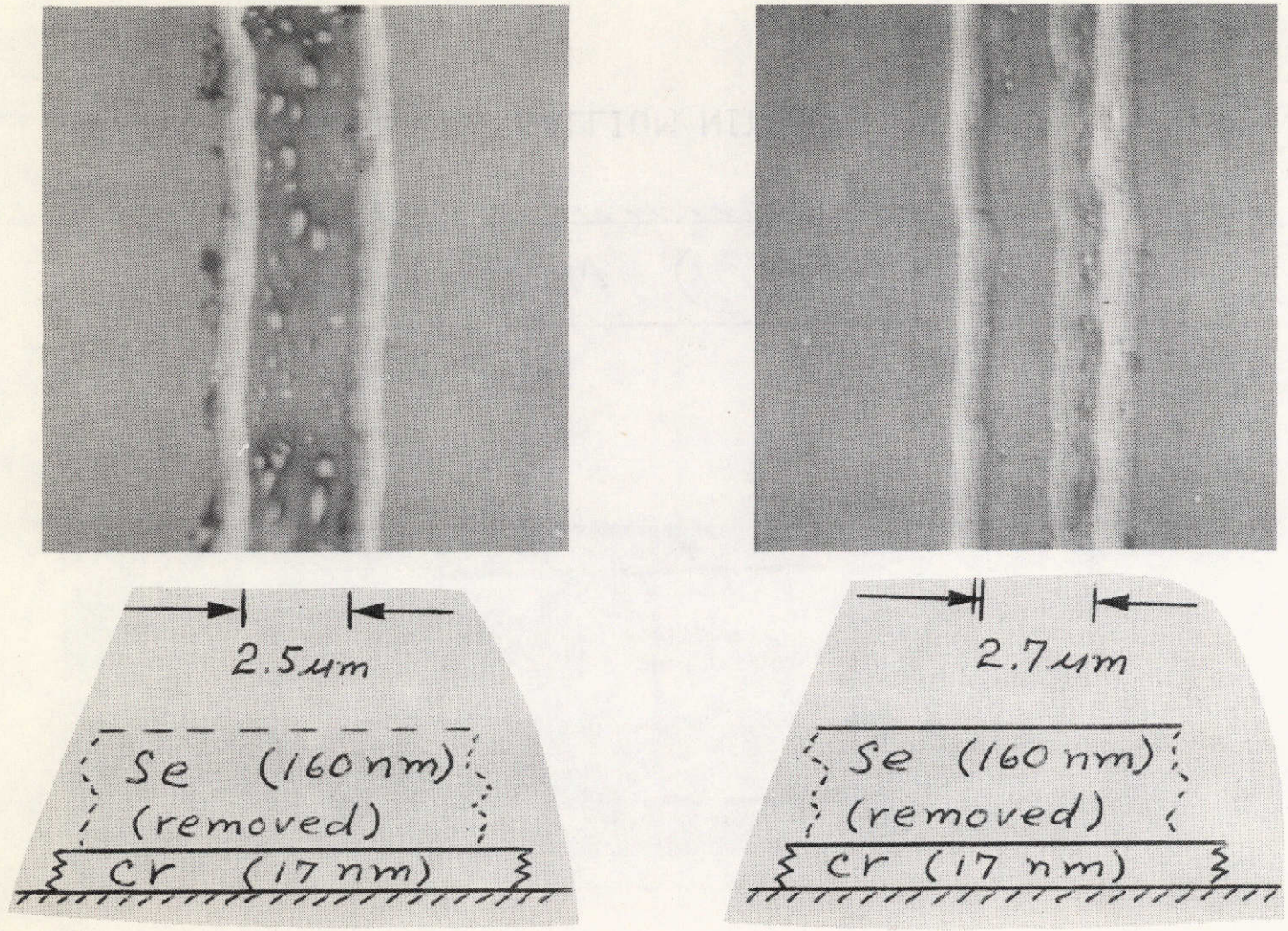

FIGURE 26 CHROMIUM

5.12 After the initial successes in getting chrome to adhere to Cer-Vit through a selenium mask, problems of poor adhesion arose, apparently because of a residue in the scribed lines. To help remove the residue, an undercoat of absorptive chrome was used beneath the selenium in order to elevate the temperature at the base of the scribed lines. Line uniformity (Figs. 23 & 24) appeared good, but except in a few instances, adherence of a chrome overcoat remained poor. Attempts to clean the lines in a glow discharge were largely unsuccessful and results were not repeatable. On one occasion, silver adhered to the Cer-Vit substrate but not to the selenium mask, and on another occasion the reverse occured. Eventually, it was concluded that selenium had contaminated the vacuum system to the point where heat from the evaporation circuits and/or from the glow discharge was subliming selenium back into the scribed lines. Cleaning the bell jar and sanding of the interior of the vacuum chamber failed, however, to restore adhesion of the chrome.

5.13 Two final experiments were undertaken using Zinc Sulfide (ZnS) and Gallium Nitride (GaN) which both sublime at 1 atmosphere of pressure. ZnS sublimes at 1180°C and GaN sublimes at about 800°C. Both are slightly absorbent to visible light. Lines scribed through a masking layers of ZnS $\frac{\lambda_o}{4}$ thick were very ragged. Similar lines scribed in GaN (Fig. 25) were also very ragged.

5.14 At the conclusion of the scribing experiments, it was observed that, in a few places, lines had been scribed not only through a layer of selenium but had melted through a 17nm thick chrome undercoat as well. Electron micrographs (after removal of the selenium) are shown in Fig. 26. One sample shows many droplets within the scribed line and the other shows a doubling of one edge of the line. The later sample is quite free of droplets. This indicates that a search for a masking material which melts cleanly might be more fruitful than the present search for a masking material that evaporates cleanly.

6. DISCUSSION

6.1 The turntable design appears to be entirely practical for versions 3 or 4 meters in diameter. Although the mass of the turntable will prevent jitter, a belt drive may be substituted for the friction wheel drive in order to provide the smoothest possible action.

6.2 The basic design of the carriage motion appears to be practical for use with interferometric control. A fine motion of the scribing lens and retroreflector assembly (Fig. 2) would be added for interferometric control. A piezoelectric actuator, controllable to $\pm .05\mu m$, would be suitable. Roller bearings would be substituted for the slide bearings to reduce hysteresis in the carriage motion to a value within the range of the fine motion (e.g. $\pm 2\mu m$).

6.3 The focal control sensor appears to be suitable for use with practically any non-diffusing mirror coating. The focus control arm also appears to be a practical mechanism. Its range ($> 100\mu m$) is sufficient to accommodate a reasonable error in the adjustment of the mirror on the turntable and its sensitivity is fully compatible with the depth of focus (approximately $\pm .5\mu m$) of the scribing beam.

6.4 The stepper motor actuator for the focus control arm is unsuitable and, in any future system, should be replaced with a hydraulic actuator. Even if the structure were stiffened to give satisfactory focal control, vibration from the stepper motor would probably interfere with the interferometric radial control. In view of the extremely low acceleration in the focal direction and in view of the fact that controllability to within 1/2% of the range is satisfactory, no serious problem with a hydraulic actuator is foreseen. Performance of the present actuator indicates that a hydraulic actuator could readily accommodate a tangential tilt error of 15 arc seconds in the mirror surface at the expected scribing speed of approximately 1.5m/sec.

6.5 For generating Type B zones, the results in Fig.26 indicate that a search for a masking material which melts cleanly might be more fruitful than the present search for a masking material which evaporates cleanly. Surface tension of the melted material might provide the deep, steep sides which evaporation has not produced. The $\lambda_o/4$ overcoat layer would then be discontinuous (or nearly so) at the edges of the scribed line

so that clean separation of the $\lambda_o/4$ layer would occur at the edges of the line when the underlying masking layer is removed.

6.6 No measurements of light scatter were made in this investigation. However, in Type B zones, if droplet size does not exceed the $\lambda_o/4$ step height of the zones, coherent diffraction produced by the zones necessarily will far exceed incoherent scatter from small droplets.

6.7 In Type A zones, droplets are a more serious matter because droplet size is likely to exceed the step height of the zones by a factor of 10 or more. In this case droplets of masking material must be removed from the final product. Zinc appears to be a promising candidate for a masking material. It scribes quite cleanly and it can be dissolved both in acids and alkalis or, if heated, it can be removed by evaporation in a vacuum.

7. CONCLUSIONS

7.1 The basic turntable design would be practical for diameters up to 3 or 4 meters.

7.2 The basic design for the radial motion of the "laser stylus" likewise would be practical. Interferometric control must be added.

7.3 The focus sensor is entirely satisfactory for a flat, uncoated surface. It is expected to operate satisfactorily on curved, coated surfaces.

7.4 Stepper motor actuation of the focus control is not satisfactory. Hydraulic actuation would be satisfactory.

7.5 A scribing speed of the order of 1.5m/sec is practical both from the mechanical standpoint and from the standpoint of laser power requirements.

7.6 For scribing Type B zones, no suitable masking material has been found. Selenium may be a practical masking material if handled under appropriate thermal conditions. Its tendency to sublime slowly in vacuo, however, has thus far frustrated all attempts to use it in this manner. Its toxicity is also a severe drawback. The prospect of finding a masking material which melts cleanly (without droplets) is perhaps better than that of finding a masking material that evaporates without a residue.

7.7 For scribing Type A zones, prospects are good that a suitable masking material could be found. Zinc is a promising candidate.

8. ACKNOWLEDGMENTS

The author wishes to acknowledge the able assistance of Mr. Roland Francois and Mr. Henry Adels.